Spectral Analysis of Ship-Based Eddy Covariance Data

by

Rui Zhang

A Thesis submitted to the Faculty of Graduate Studies of

The University of Manitoba

In partial fulfillment of the requirements of the degree of

MASTER OF SCIENCE

Department of Electrical and Computer Engineering

University of Manitoba

Winnipeg

ABSTRACT

Because of complications associated with ship motion and airflow distortion, eddy covariance (EC) from ships has not seen widespread application. In 2011, high frequency (10 Hz) measurements of three-dimensional wind velocity, temperature, CO_2 and humidity and slow response sensors recording air temperature, humidity, wind speed/direction, surface temperature were deployed on a tower installed on the foredeck of the research ice breaker *CCGS Amundsen* to characterize the surface fluxes within the Canadian Arctic Archipelago. The ensemble averaged co-spectra for wind, temperature and CO_2 showed general agreements evaluated against theoretical curves (Kaimal et al. 1972). Port- and starboard-side co-spectra appear to follow the theoretical curves while an over-estimation was seen at high frequencies for winds coming over the bow. Fluxes were also compared against modern parameterizations for CO_2, heat and momentum exchange for open water environments. The range of EC momentum and sensible fluxes looks reasonable while CO_2 flux exhibits uncertainties.

ACKNOLEGEMENTS

First and foremost, I would like to express my deepest gratitude to my advisor Dr. Gabriel Thomas and co-advisor Dr. Tim Papakyriakou for their incredible patience and expert guidance over the course of the completion of this project. I also wish to thank my committee members, Drs. Jun Cai and Jens Ehn for their support.

I would like to extend my thanks to Sebastian Luque and Meredith Pind for the help of field and lab work.

This project would not have been possible without the funding of ArcticNet, the Natural Science and Engineering Research Council (NSERC) and the University of Manitoba's GETS program.

Last but certainly not the least, I wish to thank my friends and family for the constant support and encouragement.

DEDICATIONS

To my parents, for their love and support along the way.

TABLE OF CONTENTS

LIST OF TABLES

LIST OF FIGURES

1. INTRODUCTION

1.1. BACKGROUND

At its core Arctic amplification (Manabe and Stouffer 1980), a phenomenon that global climate change is enhanced in the Arctic relative to the rest of the world, results from changing energy and mass fluxes at the surface associated in many respects to a severe reduction in sea ice extent and thickness (Polyakov 2002; Serreze and Francis 2006; Serreze et al. 2009; Screen and Simmonds 2010; Serreze and Barry 2011). A surface flux dataset over a range in ice and ocean conditions experienced in the Arctic is essential toward understanding the response of fluxes to system level changes and to validate and constrain parameterizations used in atmosphere and ocean models at all spatial scales (Andreas et al. 1979; Bates et al. 2006; Takahashi et al. 2009; Rysgaard et al. 2012; Bourassa et al. 2013).

The air-sea fluxes of heat, momentum and CO_2 respond to near surface gradient of respectively temperature, wind speed and CO_2 concentration (Liss and Slater 1974). Changes in the sea ice cover are expected to change and air-ocean exchange of momentum, heat (Screen et al. 2013) and climate relevant gases, including CO_2 (Parmentier et al. 2013).

1.1.1. *SENSIBLE HEAT FLUX*

Laikhtman and Klyuchinikova 1957 stated that great vertical temperature gradients would result in very large sensible heat fluxes. The extreme 20-40°C ocean-atmosphere temperature difference in the winter allows for strong heat exchange (Andreas et al. 1979;

Andreas and Murphy 1986). Leads and polynyas, referring to areas of open water or thin ice surrounded by thicker ice (Andreas and Cash 1999), are dominant on turbulent heat exchanges. In the winter, leads cover only 1-2% of the Arctic Ocean but contribute 70% of the upward heat fluxes (Marcq and Weiss 2012). The decreasing trend of Arctic sea ice extent enhances the rise in sea surface temperature (SST) (Serreze et al. 2009). The thinning sea ice and snow cover also account for an overall increased upward heat flux in the fall, as a result of decreased insulating effect (Kurtz et al. 2011).

1.1.2. *CO_2 Flux*

The Arctic Ocean is regarded as a profound CO_2 sink, contributing 5-14% to the global balance of CO_2 sinks and sources (Bates and Mathis 2009). Numerous physical, biological and chemical factors, such as, freshwater input, phytoplankton primary production and sea ice formation and melting (Rysgaard et al. 2011) can impact the Arctic Ocean CO_2 air-sea gas interactions (Bates and Mathis 2009). The diminishing sea ice caused by climate change is assumed to increase the capacity of atmospheric CO_2 uptake by the Arctic Ocean surface (Bates and Mathis 2009). The carbon cycle of the Arctic is being altered by the rapid change happening in the Arctic (Parmentier et al. 2013). However, the complex CO_2 dynamics is not fully understood and requires accurate measurements.

1.1.3. *The EC Application*

Eddy covariance (EC) is considered to be the only direct and well-developed method to perform flux approximation. The concept of EC first appeared more than 60 years ago

(Montgomery 1948; Obukhov 1951; Swinbank 1951) and was originally developed for heat and water vapour (Montgomery 1948; Swinbank 1951). Initially, Montgomery (1948) made use of an open system to assess heat flux. Swinbank (1951) estimated heat and water vapour fluxes with the aid of hot-wire anemometry (Obukhov 1951; Ower and Pankhurst 1977) to measure vertical wind fluctuations. With the introduction of modern fast response sonic anemometers and the emerging of infrared gas analyzers, the EC method has become a more robust method and has been applied to evaluate trace gas fluxes, particularly CO_2 (Ohtaki and Matsui 1982). However, the integration of gas analyzers as part of both open-path and closed-path EC systems for CO_2 flux requires considerable attention to system design and data processing (Leuning and Moncrieff 1990). Parameterization methods for flux estimates are not well-understood and vary in different time and space scales (Blanc 1985; Kondo and Tsukamoto 2007). Sea ice in high latitudes adds uncertainty to parameterization. Considering these concerns, currently the high precision of the EC technique is greatly appreciated.

The EC technique has been in widely uses over wide temporal and spatial scales over a variety of platforms in diverse surface conditions. To use this technique over water, experiments need to be conducted from a ship, drifting spar or moored buoy (Blomquist et al. 2014). Early shipboard measurements of momentum, sensible heat and water vapour fluxes used three-dimensional sonic anemometer and a fine-wire thermocouple psychrometer (Mitsuta and Fujitani 1974; Fujitani 1981). The attempts were successful but it has also been pointed out that apparent errors may occur due to platform motion (Mitsuta and Fujitani 1974) and flow distortion (Yelland et al. 1998 & 2002; Moat et al. 2005 & 2006; Popinet et al. 2004; Landwehr et al. 2015; O'Sullivan et al. 2013).

Correction schemes for ship motion have evolved (Miller et al. 2008; Schulz 2005; Pedreros 2003; Edson et al. 1998; Fujitani 1981; Mitsuta and Fujitani 1974), through application to various field experiments. In 1974 and 1975, during the AMTEX field programs, the EC technique was applied aboard the *R.V. Keif*u-*Maru* over the East China Sea (Fujitani 1981). Vertical translational velocity caused by ocean swell induced heaving ship movement was brought into the correction scheme and the resulting EC momentum, sensible heat and water vapor fluxes were compared with bulk parameters (Fujitani 1981). Edson et al. 1998 also showed close agreement focusing on momentum fluxes obtained using the two methods on data collected over several ship-based field programs. Subsequently, improvements have been made in later field experiments (Edson et al. 1998; Miller et al. 2008; Schulz et al. 2005; Prytherch et al. 2015; Pedreros 2003; Landwehr et al. 2015;). There remains some uncertainty on the impact of motion correction on computed fluxes, for example Landwehr et al. (2015) suggest the classic model may contribute to an overestimation of the momentum flux. Recently Miller et al. (2008; 2010; 2016) and Landwehr et al. (2015) present an evolution to traditional motion correction scheme that appear resulting in good agreement between EC-derived fluxes, and those estimated under ideal conditions using classic bulk solutions to fluxes of momentum, heat, and CO_2. The application of ship-based EC toward the calculation of fluxes for trace gases, like CO_2, is relatively new when compared to its application for fluxes of heat and momentum. McGillis et al. (2001) reported the first ship-based EC flux estimates of CO_2 from measurements made in the North Atlantic during the GasEx-98 cruise in early summer of 1998. In that study good agreement was observed between EC-derived and bulk models for CO_2 transfer velocity, particularly for wind speeds less than

11 m/s (McGillis et al. 2001). Since, there have been other important studies. In the August of 2005, the EC flux system was installed onboard the *R/V MIRAI* of JAMSTEC for CO_2 flux observations in the equatorial Indian Ocean (Kondo and Tsukamoto 2007). Measurements were made using open-path LI7500 under conditions of both small air-sea differences in partial pressure CO_2 (ΔpCO_2) and light winds and the authors observed EC-derived downward CO_2 fluxes to be orders of magnitude larger than bulk derived CO_2 fluxes in one of their stations (Kondo and Tsukamoto 2007). The discrepancy was attributed to the open-path sensors' cross-sensitivity to water vapour fluctuations and was assumed to by hygroscopic particles on the sensor lens (Prytherch et al. 2010). Weiss et al. (2007) reported EC momentum, sensible and latent heat and CO_2 fluxes measured by an open-path eddy covariance system for a one and half years observation in the Baltic Sea. Large deviation in CO_2 flux was found for wind speeds (U_{10}) greater than 10 m/s when compared to bulk parameterizations. They concluded that the reasons for the deviation were that CO_2 transfer velocity k should not solely decided by wind speed and pCO_2 measured in the air and in the water is separated. Errors may also arise from platform motion and non-homogeneity and non-stationarity of the surface layer (Weiss et al. 2007).

Early attempts to characterize the effects of flow distortion from ship-based measurements are attributed to Oost et al. (1994); Yelland et al. (1998); Dupuis et al. (2003). Booms, masts, nearby sensors, tower and other kinds of supporting and associating installation in field experiments introduce distortion (Deyer 1981; Coppin and Taylor 1983; Miller et al. 2010), affecting measured wind fields. A more severe scenario is when experiments are carried out on a big vessel. The vessel's hull and superstructure

could contribute to both mean and turbulence flow distortion (Edson et al. 1998; Pedreros 2003) and affect the EC estimate for turbulent fluxes. It is generally believed that the application of the technique for momentum flux is more strongly affected by flow distortion relative to the fluxes of heat or trace gases, largely because unlike for the fluxes of scalar quantities, the fluctuations in both the vertical and horizontal wind components are used in the determination of the momentum flux (Edson et al. 1998; Pedreros 2003; Miller et al. 2010). Edson et al. (1998) indicated that the EC-derived momentum flux could be overestimated by as much as 15% on large vessels due to flow distortion. The magnitude of flow distortion has been shown to vary by wind direction relative to the ship's bow rather than sea states (Yelland et al. 1998; Popinet et al. 2004; Landwehr et al. 2015; O'Sullivan et al. 2013). Yelland et al. (1998) found that airflow was decelerated by 4%-14% and displaced by approximately 1 m vertically and the resulted drag coefficient overestimated by as much as 60%. Popinet et al. (2004) confirmed that strong flow distortion could be caused by tiny structural components and observed up to 40% normalized standard deviation associated with not well-exposed instruments. O'Sullivan et al. (2013) showed evidence that flow distortion scales as the measured wind speed increases, however not linearly. The flow distortion error was no greater than 12% when the CFD algorithm was applied.

Considerable work has gone into the derivation of indirect flux estimates like the bulk formulations (Liss and Slater 1974; Smith 1988; Wanninkhof 1992; Wanninkhof and McGillis 1999; Fairall et al. 2003; McGillis and Wanninkhof 2006; Andreas et al. 2008; Nightingale et al. 2000; Wanninkhof et al. 2009) to the point where the community has reasonable confidence in flux results in open seas, particularly for fluxes of heat and

momentum (Pond et al. 1971; Blanc 1985; Andreas and Murphy 1986; Andreas et al. 2008; Edson et al. 1998 & 2013). There is also reasonable confidence in the bulk parameterization of CO_2 flux under specific conditions (Brunke et al. 2006; Bourassa et al. 2013) based on measurement of the air-sea difference in the partial pressure of CO_2 (ΔpCO_2) and transfer velocity, usually made a function of wind speed, seawater temperature and salinity. Concerns exist as to how well current transfer velocities represent processes of exchanges of momentum and gases (Bourassa et al. 2013), and measurements of ΔpCO_2 based on measurements of seawater pCO_2 metres from the sea surface, as is the case on most ship-based experiments (Takahashi et al. 2002; Butterworth and Miller 2015). Surface pCO_2 could be considerably different than that measured 3-5 m beneath the surface in the presence of strong stratification in the upper mixed layer associated with freshwater from ice melt (sea ice or glacier), or river inflow (Geilfus et al. 2015). Bulk-style parameterizations for heat and momentum over sea ice have been developed (Weeks 2010; Bourassa et al. 2013), but have not been extensively tested. The representation of these fluxes over complex surfaces of mixed ice-ocean have not been extensively tested (Geilfus et al. 2014). Several studies have documented an exchange of CO_2 over sea ice, although there remains considerable uncertainty on the flux magnitude and variability owing to a discrepancy in fluxes arising from chamber measurements and micrometeorological techniques like EC (Comiso et al. 2008; Rysgaard et al. 2011). Very few flux measurements have been published over polar seas and with variable ice coverage (Tison et al. 2002; Rysgaard et al. 2011; Geilfus et al. 2014). Loose et al. (2014) present a parameterization for air sea CO_2 in such environments, yet it remains largely untested. Recently, Butterworth et al. (2016)

observed good agreement between EC-derived estimates for heat, momentum and CO_2 and bulk-style estimates.

1.1.4. *THESIS OBJECTIVES*

The primary objective of this thesis is to evaluate the performance of the EC system on the medium size icebreaker *CCGS Amundsen* for determining fluxes of momentum, heat and CO_2 over a wide range of conditions and better understand challenges of ship-based flux measurements in the changing Canadian Arctic Archipelago.

Considering the issues that we may encounter from ship-based measurements, specifically our goals are as follows:

1) Implement motion correction routine and make necessary adjustments.
2) Perform quality control by general meteorology as well as from the co-spectra perspective (comparing against theory).
3) Examine resulting fluxes by comparing against bulk-derived fluxes.
4) Identify and discuss potential problems and make reasonable corrections.

1.2. THEORY

1.2.1. *THE EC THEORY*

The application of this EC technique is dependent on the validity of several assumptions, including that there be negligible density fluctuations, flow convergence and divergence is negligible, horizontal homogeneity in surface properties and measurements are stationary and made within the surface layer (Burba and Anderson 2010). It follows that fluxes are estimated for sensible heat (H), latent heat (LE),

momentum flux (τ) and CO_2 (F_c) using the following equations respectively (Stull 1988; Foken 2008):

$$H = \rho C_p \overline{w'T'}, \quad (1)$$

$$LE = L_v \rho \overline{w'q'}, \quad (2)$$

$$\tau = -\rho \overline{w'u'}, \quad (3)$$

$$F_c = \rho \overline{w'c'}, \quad (4)$$

where the product with overbar represent the covariance of fluctuations (denoted by prime) in vertical velocity (w) and scalar (T=temperature, q=specific humidity, c is CO_2 mixing ratio), or horizontal wind speed (u) as required for the momentum flux. In Eq. (1) to (4), ρ is the mass density of air, C_p is the specific heat capacity of air at constant pressure and L_v is the latent heat of vaporization of water.

Spectral analysis is often used to assess the EC system's performance and identify sources of potential bias. The contributions from eddies of various sizes to the overall flux are clearly reflected in the shape of the co-spectra. Making use of signal frequency decomposition, the distribution of covariance into different frequency bandwidth represents eddies of various sizes. The covariance of each item is the area under the co-spectral curves. Similarly, the variance of the quantity of interest λ is the integration of the power spectra of that quantity:

$$\overline{\lambda'^2} = \int_0^\infty S_\lambda(f) df, \quad (5)$$

$$\overline{w'\lambda'} = \int_0^\infty Co_{w\lambda}(f) df. \quad (6)$$

There are a variety of presentations for turbulence spectra and co-spectra analysis. The basic linear-linear plot is seldom used because the range of data is too wide to be clearly displayed. Often seen is the log-log presentation. When $\log [S(f)]$ is plotted

against f, the -5/3 slope in the inertial sub-range can be shown. Another widely used presentation is the log-log graph on normalized spectra and normalized frequencies. When the spectra are frequency weighted by natural frequencies, they have the same unit as the variances. Hence, $fS(f)/var$ is the non-dimensional form of the spectra.

Much of our empirical understanding on the application of spectral analysis for fluxes in the surface layer is attributed to the Kansas experiment (Kaimal et al. 1972). Associated data provided empirical normalized power spectra and co-spectra for wind velocity and scalars as functions of z/L under ideal conditions. The spectra and co-spectra plots in a log-log scale imply that when normalized spectra and co-spectra are plotted against normalized frequency, spectral peaks are shifted towards higher frequencies when stability increases (Kaimal et al. 1972). Another noticeable characteristic is in the inertial sub-range, defined as the region separating the energy containing and dissipation ranges, the spectra and co-spectra decrease following constant slopes and this is known as the famous Kolmogorov's 5/3 law (Kolmogorov 1941).

1.2.2. *Other Micrometeological Quantities*

Turbulent momentum flux, also called Reynolds stress (τ_R), is the rate of air travels across the measurement surface (Stull 1988). The measurement of τ_R is the friction velocity (u_*), one of the most important scaling variables. The square of friction velocity is calculated as (Stull 1988):

$$u_*^2 = |\tau_R|/\bar{\rho}, \tag{7}$$

where $\bar{\rho}$ is the air density. Another form of friction velocity defined as a function of the covariance is:

$$u_*^2 = (\overline{uw}^2 + \overline{vw}^2)^{1/2} \quad (8)$$

The dynamical properties are described by Monin-Obukhov similarity theory (Stull 1988). It is extensively used and serves as the base of many flux estimation techniques. The Monin-Obukhov stability length *L* that describes the effect of buoyancy on the total turbulent kinetic energy is calculated as:

$$L = \frac{u_*^3 T_0}{g\kappa \overline{w'\theta_v'}} \quad (9)$$

where T_0 is a reference temperature, g is gravitational acceleration, κ is the von Karman constant, and $\overline{w'\theta_v'}$ is the flux of virtual potential temperature θ_v (Kaimal et al. 1972; Sørensen & Larsen, 2010). The ratio z/L is the stability parameter representing the normalized buoyant production or loss. z/L is positive when the atmosphere is stable, negative when unstable and close to zero under neutral conditions (Stull 1988).

Turbulent kinetic energy (TKE) is an important term in meteorology that represents the intensity of turbulence. TKE per unit mass (m) is quantified by the turbulent stress (Stull 1988):

$$\frac{TKE}{m} = \frac{1}{2}(u'^2 + v'^2 + w'^2) \quad (10)$$

1.2.3. *Bulk Methods*

The principle guiding the bulk approach over the air-sea interface is the relationship

$$F_x = C_x \, \Delta X \quad (11)$$

where C_x is the transfer coefficient of the entity x and ΔX is the difference of concentration in the sea and in the atmosphere (Fairall et al. 2000). The momentum flux (τ) is parameterized as:

$$\tau = \rho C_d \overline{U}^2 \quad (12)$$

with C_d being the drag coefficient. And the sensible heat flux is determined as:

$$H = \rho C_p C_H \overline{U}(\theta_s - \theta_a) \quad (13)$$

where C_H is the exchange coefficient for heat, θ_s and θ_a are the surface and near surface air temperature.

The bulk CO_2 flux, can be empirically calculated as:

$$F_{CO_2} = k_{CO_2} K_0 \Delta pCO_2 \quad (14)$$

where K_0 is the solubility of seawater to CO_2, dependent of temperature and salinity, k_{CO_2} is the transfer velocity of CO_2, and ΔpCO_2 is air-sea difference in partial pressure of CO_2 in (Weiss 1974; Wanninkhof et al. 2009; Mørk et al. 2014). Several parameterizations for K_0 have been proposed and the commonly used ones are from Wanninkhof (1992), Wanninkhof and McGillis (1999) and Weiss et al. (2007). The transfer velocity of CO_2 (k_{CO_2}) is dependent on wind speed. The difference of CO_2 partial pressure (ΔpCO_2) is determined primarily by the partial pressure in the seawater (pCO_{2sw}), as there is very slight variation of CO_2 concentration in the atmosphere (pCO_{2atm}) globally. Positive (negative) CO_2 flux represents fluxes from the ocean (atmosphere) to the atmosphere (ocean), indicating the ocean as a CO_2 source (sink).

1.2.4. *Instrumental Methods*

Modern ship application of the EC method requires a fast response three-dimensional sonic anemometer, an infrared gas analyzer (IRGA), and to account for platform motion, a motion sensor is needed to collect information on the linear accelerations and angular rates of the platform. The motion of a ship has six degrees of freedom and can be decomposed into translational motion and rotational motion. Translational movement

includes up and down movement (heave), left and right movement (sway) and forward and backward movement (surge), and rotational movement involves forward and backward tilt (pitch), side-to-side tilt (roll) and turning left and right (yaw).

The three-dimensional wind velocity is measured by sonic anemometers and is vulnerable to biasing effects. Angle of attack is defined as the arctangent of vertical wind velocity over horizontal wind velocity and indicates the imperfect response of the anemometer (Gash and Dolman 2003; Nakai et al. 2006). This effect is inevitable due to the presence of the anemometer frame and the transducers (Kaimal and Finnigan 1994; Gash and Dolman 2003; Nakai et al. 2006), but also can be exasperated by the distortion of flow by ship superstructure. An axis rotation can be applied to compensate for both the effects of motion, and deflection of the air stream angle of attack. Wind tunnel experiments show that fluxes are largely underestimated when angles of attack are significant and the magnitude of error was proved to rely on wind direction (Molen et al. 2004). Gash & Dolman (2003) named the sine error in the vertical wind conponent along with the cosine errors in the horizontal component as the (co)sine error. Outside the optimal angle of attack range, the performance of anemometer degrades and results in underestimated turbulent fluxes (Van Der Molen, Gash, and Elbers 2004; Cava et al. 2008). The correction was derived for the R2 and R3 type anemometers and is suggested to be performed as part of the correction routine on raw data (Molen et al. 2004).

Infrared gas analyzers (IRGAs) are capable of returning CO_2 and H_2O concentrations. Two classes of sensors are widely used, open-path and closed-path. With the closed-path system a tube intake is placed in close proximity to the sonic anemometer and air is drawn through the tube and into the measurement chamber of the sensor. The open-path

sensor itself can be situated in close proximity to the sonic anemometer allowing for measurement of gas concentration without the use of an intake tube. However, neither open-path nor closed-path measurements in marine environments are perfect. Open-path offers advantages over closed-path design in the aspects of eliminating tube attenuation effects and averting time lags (Leuning and Judd 1996). In the meantime, it suffers from contaminants, such as sea spray, precipitation, dew and fog. For open-path systems, the WPL (Webb, Pearman, and Leuning 1980) density correction needs to be applied to compensate for the biasing effects on the CO_2 flux associated with fluctuations in water vapour density, temperature and pressure (refer to section 1.4.3). Salt contamination is another source of error that affects water vapour density measurements (Bradley and Fairall 2006). Thus the sensor heads need to be cleaned frequently to keep the hazards to the lowest level. For the closed-path system, these humidity and temperature density fluctuations effect is less than that experienced by the open-path system and can be accounted for by converting CO_2 density or mole fraction to mixing ratio (Lee et al. 2005). However, the analyzer used in the closed-path system is prone to platform motion (McGillis and Edson 2001). This bias can contribute 30% of the true CO_2 flux according to McGillis et al. (2001). Another density impurity arises from the cross-sensitivity to water vapour (Kohsiek 2000) and salt (Prytherch et al. 2010) experienced by the open-path sensor and can cause an overestimation of CO_2 fluxes an order of magnitude greater than expected (Prytherch et al. 2010). This water vapour crosstalk effect is more prominent in the situation of small CO2 flux and high humidity and was also seen in the measurements using the closed-path system LI7200 (Blomquist et al. 2014). The LI-COR embedded correction algorithm is still inadequate when CO_2 flux is small while H_2O flux

is large and could result in significant error in the computed CO_2 flux (Blomquist et al. 2014; Edson et al. 2011).

Tracing down the history of instrumental approaches for IRGAs over the past decades, open-path sensors tend to be in more widespread use (Blomquist et al. 2014). Observations suggest that the open-path sensor is less affected by ship motion prompting Miller et al. (2010) to effectively integrate open-path sensors into a closed-path system, thereby taking advantages of both open-path and closed-path designs. A cylindrical glass cell was inserted into the optical path, thus the open-path CO_2 IRGA (LI7500) was configured to closed-path (Miller et al. 2010).

1.3. SHIP APPLICATION AND CHALLENGES

1.3.1. *MOTION CORRECTION CHALLENGE*

The first issue with ship-based measurements is the need of correction for instrument offsets, wave-induced tilt, rotation as well as ship speeds and heading (Edson et al. 1998; Miller et al. 2008). Ship motions are defined by the six degrees of freedom continually measure by the motion sensor. Motion contamination results from: 1) instantaneous tilt of the anemometer due to pitch, roll, and yaw of the vessel; 2) rotational movement at the anemometer about its local coordinate system axes; and 3) linear movement of the platform with respect to a fixed frame of reference (Hare et al. 1992; Edson et al. 1998).

Problems not only occur in momentum flux, motion also interference with certain IRGA measurements, resulting in imprecise CO_2 and H_2O concentrations (Blomquist et al. 2014). Errors may also occur due to mechanical sensitivities of the sensors as well as

the hydrostatic pressure fluctuation due to with ship heave (McGillis et al. 2001; Yelland et al. 2009; Miller et al. 2010; Prytherch et al. 2015).

1.3.2. *Flow Distortion Treatment*

During the past few decades, much effort has been made to combat flow distortion. The generally accepted method is to put limits on relative wind direction (**Table 1**). A good compromise to avoid flow distortion is the indirect ID (Pond et al. 1971; Fairall and Larsen 1986; J. B. Edson et al. 1991; Anderson 1993) and the CSP (Sørensen and Larsen; Norman et al. 2012) methods mentioned previously, alternatively, some researchers have tried to quantify the effects of distortion. Wind tunnel simulations showed a non-zero upward vertical deflection for all wind directions and specific correction factors then were derived (Barlow et al. 2011). Other investigators determine and correct for flow distortion by simulating flow using three-dimensional computational fluid dynamics (CFD) modeling over individual platforms (Yelland et al. 1998; Yelland et al. 2002; Moat et al. 2006). Yelland et al. (1998) modeled acceleration and vertical displacement of the flow using CFD and found an overestimation of the drag coefficient by approximately 60%. However, both wind tunnel simulations and the numerical CFD simulations were derived for specific experiments and yet no universal approach has been reached. Landwehr et al. (2015) argued that the classic approach can lead to large overestimation of fluxes because of unreliable wind vector tilt and proposed a new scheme for measurement made on mobile platforms. This novel method suggests applying the tilt correction before correcting for the mean ship velocity and was proved to have improved the previous correction for flow distortion and motion.

Table 1. List of restrictions on relative wind direction on different platforms

	Song et al. 1996	Edson et al. 1998	Pedreros 2003	Miller et al. 2008	Prytherch et al. 2015
Marine Platform	R/V *Kexue* #1	R/V *Iselin*	R/V *L'Atalante*	R/P *FLIP*	RRS *James Clark Ross*
Range of relative wind direction	±45°	±60°	±30°	±60°	−20°/+50°

1.4. DATA POST-PROCESSING STEPS

1.4.1. *MOTION CORRECTION*

The correction scheme for platform motion has evolved and was presented by several authors (Miller et al. 2008; Schulz 2005; Pedreros 2003; Edson et al. 1998; Fujitani 1981). Miller et al. (2008) describes a method that 1) considers mounting misalignment between the anemometer and the motion sensor; 2) selects a higher order Butterworth filter which could lessen the "leakage" between the low and high frequency Euler angles. In Miller et al. (2008), the anemometers were mounted on the portside boom 20 meter off the research platform R/P *FLIP*. In such mounting, the misalignment between the anemometer and the motion sensor need also be corrected for and the correction was proved to contribute one-third of the total motion correction (Miller et al. 2008).

1.4.2. *COORDINATE ROTATION*

To align wind speeds measured from a sonic anemometer to the local mean streamline coordinate system, coordinate rotation needs to be applied. In the natural wind coordinate system indicates, the x-axis holds the mean airflow. It is especially important for non-uniform and complex terrains. The merits of converting to the streamline coordinate system are to accommodate the data for further analysis and evaluate the data against theoretical model acquired over a flat topography (Wilczak et al. 2001). Commonly used methods are double rotation (DR), triple rotation (TR) and planar fit (PF). The double rotation scheme, indicated by its name is to rotate the coordinate twice, first about the z-axis and then the new y-axis, to vanish cross and vertical wind components (Kaimal and Finnigan 1994; Yuan et al. 2007). The double rotation was reported to create unrealistically large Euler angles and overestimate wind stress at low wind speeds because of diabatic effects (Wilczak et al. 2001; Liu et al. 2012). The TR method involves an additional rotation about the new x-axis so that the cross-stream stress equals zero. However, this third rotation was found to inflate the error and was not suggested to apply to marine conditions (Wilczak et al. 2001). Another flaw of the DR method and the TR method is sampling limitation and is especially prominent under light wind conditions. To resolve the above issues, Wilczak et al. (2001) proposed the PF method. The PF method computes wind stressed over the entire collection of data runs. With a much longer observational time series used, sampling error could be greatly alleviated. It should be noted that the change of the orientation of the anemometer need to be avoided during the whole experiment (Wilczak et al. 2001). Suggestion was given that the PF method instead of DR and TR should be adopted for underway measurements (Landwehr et al. 2015; Wilczak et al. 2001). It has also been noticed that the rotated

mean vertical wind components may not be zero due to the flow distortion (Wilczak et al. 2001; Miller et al. 2008).

1.4.3. *Density Correction*

Density correction needs to be performed to account for temperature, pressure and water vapor fluctuations. The WPL-type correction is typically applied for both open-path and closed-path systems (Webb et al. 1980; Leuning and Moncrieff 1990; Leuning 2004; Massman 2004; Ibrom et al. 2007). The WPL correction was developed on the assumption of zero mean vertical mass fluxes but is not necessary when gas concentrations are expressed in mixing ratio (Webb et al. 1980). The three steps to apply the WPL corrections for open-path systems are thoroughly explained in Lee et al. (2005). Ibrom et al. (2007) argued that the original WPL corrections on closed-path systems are biased because the measured concentrations cannot represent the gas concentrations in the air. They proposed a refined version of the WPL formulas applied during data processing for closed-path systems that accounts for decoupling of the water vapour and CO_2 concentrations when the raw data is not expressed in mixing ration and obtained similar results as the fluxes derived from raw data that has been case-by-case converted to mixing ratio.

1.4.4. *SND Correction*

SND correction, also called the Schotanus correction (Schotanus et al. 1983) refers to the conversion of buoyancy flux to sensible heat flux (Aubinet et al. 2012).

1.4.5. *Time Lag Compensation*

As the intake tube in a closed-path system delays the measurements of gas concentrations, time lag compensation needs to be applied. There are several options. The most intuitive approach is to compute the travel time from the volume of the tube and mean flow rate. However this method is subject to many uncertainties and is not plausible for water vapor because of its stickiness. Another commonly used method is covariance maximization (Fan et al. 1990). Within a specific search window, the covariance between vertical wind speed and gas concentrations is calculated and the time lag is determined where the maximum covariance is reached.

1.4.6. *Spectral Corrections*

Because of the inherent design of the eddy covariance system and the calculation of the flux, spectral attenuation is inevitable at both low and high frequencies (Lee et al. 2005; Burba and Anderson 2010). Thus, corrections for flux losses are recommended at both frequencies and one approach is the transfer function method (Lee et al. 2005). Moncrieff et al. (1997) presented and verified the system of transfer functions accounting for digital running mean, sensor separation, sonic path averaging, tube loss, *LI-COR* dynamic frequency response, sensor response mismatch and solent dynamic frequency response. Transfer functions correcting for flux loss at low frequency due to the finite flux averaging time, fluctuation term calculation have also been described and tested (Lee et al. 2005).

2. METHODS

2.1. MEASUREMENT METHODS

Measurements were made during the 2011 cruise (July 19, 2011 – October20, 2011) of the *CCGS Amundsen*. The ship travelled from Baffin Bay along east coast to west coast through Kugluktuk to Beaufort Sea in the summer and returned to Baffin Bay in the fall. The cruise is shown on map in **Figure 1.** Details on the measurement systems follow.

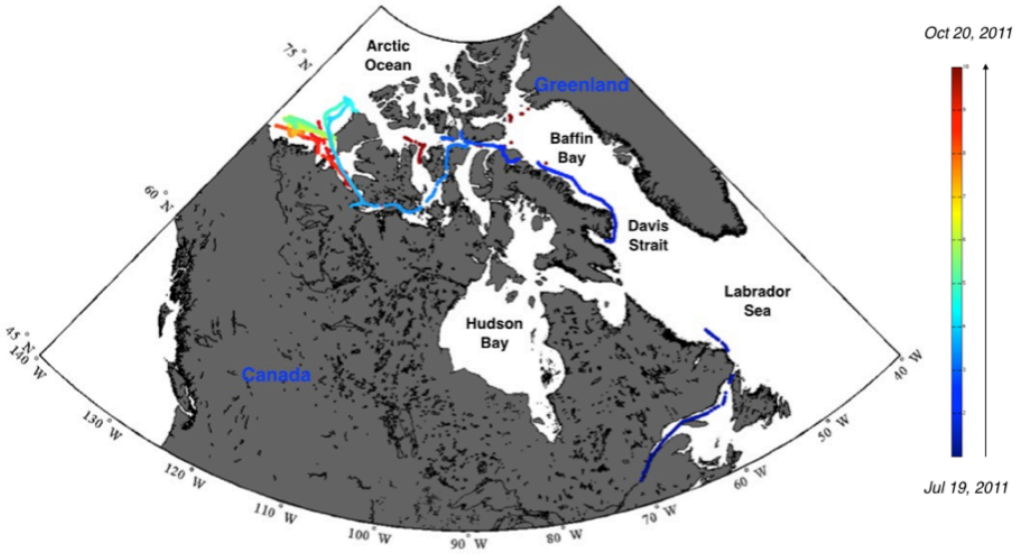

Figure 1. Ship track on map during the 2011 cruise.

Table 2. Summary of variable inventory and application

Variable	Instrumentation	Location	Purpose	Sample/Average Frequency (s)
Air temperature (Ta)	HMP45C-212	foredeck tower	General meteorology	1 / 60
wind speed (ws-2D)	RM Young 05106-10	foredeck tower	General meteorology; EC data screening	1 / 60

wind direction (wd-polar)	RM Young 05106-10	foredeck tower	General meteorology; EC data screening	1 / 60
sea surface temperature (Tsfc)	Apogee SI-111	foredeck	Bulk flux	1 / 60
ship heading (H)	OceanServer OS5000	foredeck tower	Ancillary information; Motion correction for EC flux	1 / 10
ship speed over ground (SOG)	Garmin GPS16x-HVS	foredeck tower	Ancillary information; Motion correction for EC flux	1 / 10
ship course over ground (COG)	Garmin GPS16x-HVS	foredeck tower	Ancillary information	1 / 10
ship location (latitude, longitude)	Garmin GPS16x-HVS	foredeck tower	Ancillary information	1 / 10
wind speed 3D (u, v, w)	Gill Wind Master Pro	foredeck tower	EC flux	0.1 (10 Hz)
sonic temperature (Ts)	Gill Wind Master Pro	foredeck tower	EC flux	0.1 (10 Hz)
atm. water vapour concentration (ρ_v)	LICOR LI7500 & LI7000	foredeck tower	EC flux	0.1 (10 Hz)
atm. concentration of CO_2 (ρ_c)	LICOR LI7500 & LI7000	foredeck tower	EC flux	0.1 (10 Hz)
rotational motion (accx, accy, accz, r x, r_y, r_z)	Systron Donner MotionPak	foredeck tower	Motion correction for EC flux	0.1 (10 Hz)
upper sea water temperature (Tsw)	General Oceanics 8050 pCO_2	under-way system, foreward engine room	Ancillary information; Bulk flux	3 / 60
dissolved CO_2 in seawater	General Oceanics 8050 pCO_2	under-way system, foreward engine room	Ancillary information; Bulk flux	3 / 60

(Adapted from Papakyriakou Leg 1 2011 Cruise Report)

2.1.1. *THE EC SYSTEM AND GENERAL METEOROLOGY*

A micrometeorological tower (**Figure 2**), consisting of an eddy covariance system and slow response sensors for general meteorology and bulk parameterization, was mounted on the foredeck. A summary of instrumentation associated with the systems is shown in **Table 2**. The EC facilities were firmly attached to a tower on the foredeck at the height of 14.1 m above sea level (nominal 8 m above the deck). The three-dimensional wind speed, as well as temperature was measured with the sonic anemometer *Gill Windmaster Pro*. Horizontal wind speed, T/RH and atmospheric pressure was measured at 1-second intervals and saved as 1 minute averages to micrologger (Campbell Scientific ® CR1000) using 2-D wind monitor (RM Young). A *LI-7500* (LI-COR) open-path CO_2/H_2O gas analyzer and a closed-path gas analyzer *LI-7000* (LI-COR) were used to monitor gas concentrations. Also, the air was drawn through an intake located just beneath the base of the sonic anemometer 10 m to the LI-7000 that was held in an enclosure at the base of the tower. The intake tube was heated, 10 m long, with a diameter of 6.4 mm and flow rate was on average 12 l/m. The three-dimensional accelerations and angular rates needed for motion correction were traced by the multi-axis inertial sensing system *MotionPak* (Systron Donner, Inc.). The northward, eastward and vertical separations for LI7000 reference to Gill Windmaster Pro were 10 cm, 20 cm and 15 cm respectively. MotionPak was installed 1.7 m forward and 2.725 m upward relative to *Gill Windmaster Pro*. The high frequency data needed for EC method was recorded and saved at 10 Hz and also stored as 1-minute averages on a micrologger *CR3000* (Campbell Scientific, Inc.). Additional data, such as navigation data, radiation data and sea ice information were also collected by the POS MV® inertial navigation

system onboard for the purpose of motion correction and analysis on sea ice's impact on surface gas exchanges.

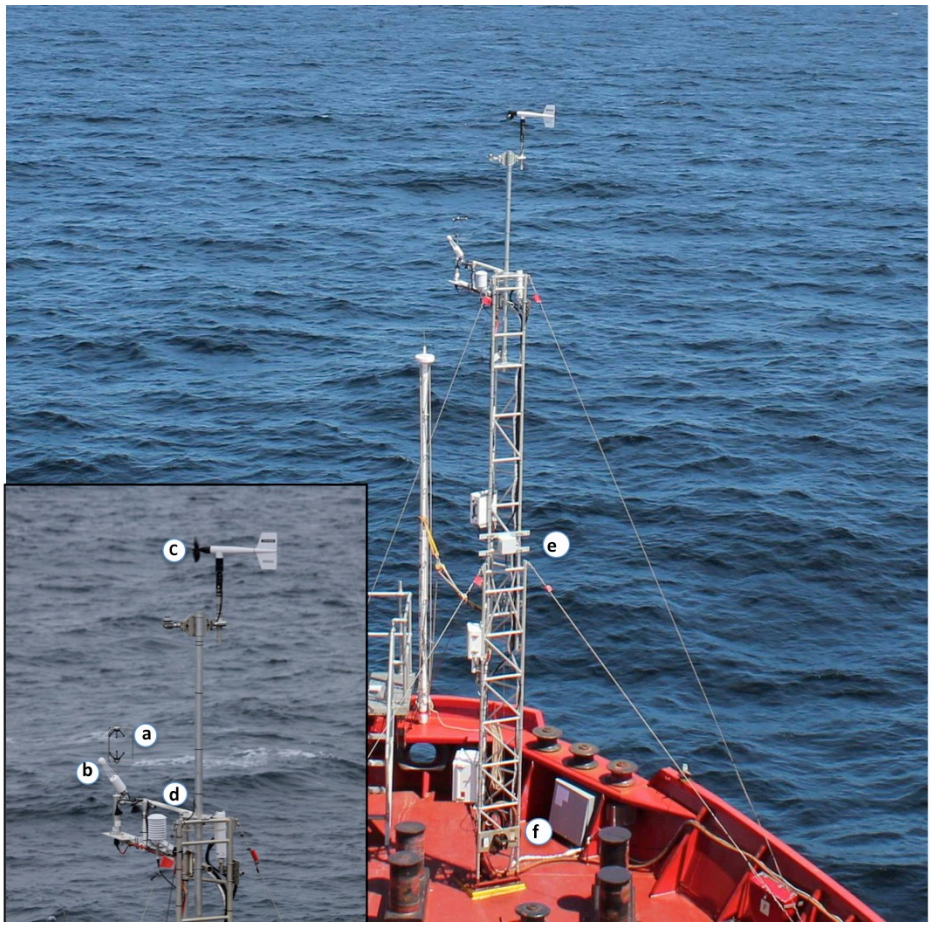

Figure 2. The meteorological tower on the foredeck of the research vessel *CCGS Amundsen* (left); Lower left corner is a close-up of the top of the tower; a) 3-D sonic anemometer (Gill Wind Master Pro); b) open-path CO_2/H_2O analyzer (LICOR 7500A); c) 2-D wind monitor (RM Young 05106); d) closed-path CO_2/H_2O analyzer intake tube; e) motion sensor (Systron Donner MotionPak); f) closed-path CO_2/H_2O analyzer (LICOR 7000).

Sea ice data were retrieved from the Canadian Ice Service in addition to manual visual observations taken from the bridge of the ship by Coast Guard and science crew and recorded in a science log. Observations were not systematically documented, and frequency ranged from half hour to several hours. Pictures were taken daily from ship's bridge and the pictures could be used to single out days when sea ice was present and days where there is open water. Science log was maintained and has the most complete information.

2.1.2. *Surface Seawater Temperature and Partial Pressure of CO_2 (pCO_2)*

A General *Oceanics 8050 p*CO_2 system (Pierrot et al. 2009) was located in the forward engine room, sampling water at a depth of 5 m with a high-volume inlet (Burgers 2015). pCO_2 was corrected for difference in temperature between water temperature at the intake and in the system's equilibrator following Takahashi et al. (1993). Additional details are available in Else et al. (2011).

2.2. Data Processing

Table 3. List of processing platforms and methods

	Platform	Method
Synchronization and splitting into 20 minutes periods	*IDL®*	
Initial screening	*IDL®*	Screening out periods with inadequate samples
De-spiking and interpolation	*IDL®*	
Motion correction	*Matlab® Version R2013a*	(Miller et al. 2008)
Angle-of-attack correction	*EddyPro®*	(Nakai and Shimoyama 2012)

	Version 6.0.0	
Axis rotation	*EddyPro®* *Version 6.0.0*	Planar fit (Wilczak et al. 2001)
Time lags compensation	*EddyPro®* *Version 6.0.0*	Covariance maximization with default (Fan et al. 1990)
Compensation of density fluctuations	*EddyPro®* *Version 6.0.0*	(George Burba et al. 2012; Ibrom et al. 2007; Webb et al. 1980)
Flux calculation	*EddyPro®* *Version 6.0.0*	(Stull 1988)
SND correction	*EddyPro®* *Version 6.0.0*	Conversion of buoyancy flux to sensible heat flux (Schotanus et al. 1983; Molen et al. 2004)
Spectral correction of high-pass filtering effects	*EddyPro®* *Version 6.0.0*	(Lee et al. 2005)
Spectral correction of low-pass filtering effects	*EddyPro®* *Version 6.0.0*	(Moncrieff et al. 1997)

To obtain EC flux, raw data was processed over different platforms. The main processing involved are motion correction, angle of attack correction, axis rotation, time lags compensation, density conversion, SND correction and spectral corrections of high-pass and low-pass filtering effects (**Table 3**). Each of the biasing effects has been previously defined.

2.2.1. *Bulk Flux (pCO_2 Correction)*

Apparent winds were converted to true winds following (Smith et al. 1999). Necessary position and heading information for the correction were acquired from the ship's GPS and POS MV® inertial navigation system.

By using a regression analysis, a strong linear correlation ($T_{sw} = 0.98*T_{eq} – 0.86$) was found between the equilibrator water temperatures (T_{eq}) and surface water temperature (T_{sw}) measured by the ship's CTD sensor (Pind, 2013). A correction on pCO_2 was made following Takahashi et al. (1993) with the linear relationship obtained. Bulk fluxes of

CO_2 were computed using the transfer velocity attributed to Wanninkhof (2014). Mean wind speed was scaled to 10-m height using the semi-logarithmic wind profile equation for the surface layer:

$$U_{10n} = \left(\frac{u^*}{k}\right) \ln\left(\frac{10}{z_0}\right), \quad (15)$$

Where $u^* = (\tau/\rho)^{1/2}$ is the friction velocity (m/s), z_0 is the roughness length, and k is von Karman's constant (0.4). The roughness length is calculated using wind data measured at two levels. Bulk fluxes for momentum, sensible and latent heat were calculated using the Coupled Ocean-Atmosphere response Experiment (COARE) 3.0 bulk parameterizations. The bulk solution to fluxes assumes open water with unlimited fetch. Fluxes were calculated using 20-minute averaged inputs (wind, temperature, CO_2 concentration).

2.2.2. *EC FLUX*

2.2.2.1. LOW-FREQUENCY WIND CORRECTION AND INITIAL PROCESSING

The initial data screening and preliminary processes was accomplished using *IDL*® scripts. Data associated with navigation (1 Hz), meteorology (0.1 Hz), radiation (0.1 Hz), 3D wind (sonic anemometer, 10 Hz), motion sensor (10 Hz) and gas analyzers (10 Hz) data were synchronized and split into 20 minutes periods for flux analysis. Data recorded while cleaning and calibrating were rejected. Preliminary processing should take place to detect and correct for unrealistic and missing samples (NANs). Periods in which 2% of the records are NANs were skipped. Spikes and remaining NAN records were spotted and filled in using shot filter. Cases when the average vertical wind speed is greater than 7m/s or/and the deviation between sonic temperature and mean air temperature is greater

than 7 degrees are considered bad sonic data and need to be eliminated. Bad motion data was when horizontal acceleration is greater than 8m/s and was also screened out. A moving average filter with a 100-sample window was applied to ship heading. Low frequency navigation and meteorology data was interpolated to match high frequency (10Hz) EC data.

2.2.2.2. MOTION CORRECTION

We adopted the conventional right-handed reference coordinate frame with the x-axis pointing to bow, y-axis to port and z-axis upward used in other studies (Fujitani 1981; Edson et al. 1998; Miller et al. 2008). Following Miller et al. (2008, and others), the three Euler angles roll ϕ, pitch θ, and yaw ψ indicates the three-seperate rotations about the x-axis, the y-axis and the z-axis in sequence. The transformation matrix T is defined as the product of the three rotation matrices:

$$T(\phi,\theta,\psi) = \begin{bmatrix} cos\psi & -sin\psi & 0 \\ sin\psi & cos\psi & 0 \\ 0 & 0 & 1 \end{bmatrix} \begin{bmatrix} cos\theta & 0 & sin\theta \\ 0 & 1 & 0 \\ -sin\theta & 0 & cos\theta \end{bmatrix} \begin{bmatrix} 1 & 0 & 0 \\ 0 & cos\phi & -sin\phi \\ 0 & sin\phi & cos\phi \end{bmatrix}. \quad (16)$$

The main equation for motion correction is

$$V_{corr} = TV_{obs} + T\left(\int \ddot{A}dt + \Omega \times R\right) + V_{ship}, \quad (17)$$

where $V_{corr} = (u_{corr}, v_{corr}, w_{corr})$ is the corrected wind vector;

$V_{obs} = (u_{obs}, v_{obs}, w_{obs})$ is the observed wind vector; T is the transformation matrix that rotates the ship frame coordinate to the reference coordinate systesm; $\ddot{A}=(\ddot{A}_x, \ddot{A}_y, \ddot{A}_z)$ is the three channel linear acceleration in ship frame; Ω is the angular rates vector also in ship coordinate; R stands for the position vector from the motion sensor with respect to

the anemometer; V_{ship} represents the velocity vector of the ship in the reference frame (Fujitani 1981; Edson et al. 1998; Miller et al. 2008).

A complimentary filter, by definition, is a combination of a low-pass and a high-pass filter. The high frequency content of the Euler angles used in the transformation matrix can be estimated based on the integration of the angular rates while the low frequency pitch and roll angles are approximated from the ratio of measured horizontal acceleration to the gravity acceleration, i.e. $\phi = arctan(\ddot{A}_y/g);\ \theta = arctan(-\ddot{A}_x/g)$ (Miller et al. 2008). The low freqeucny yaw is retained from the navigation data (Miller et al. 2008). Then the high-pass filtered integrated angular rates from the motion sensors were added together with the low-pass filtered anemometer data (Edson et al. 1998; Miller et al. 2008). The measured three-dimensional acceleration is a result of acceleration due to ship movement as well as the gravitational components. To eliminate these tilt-induced gravational components, Miller et al. (2008) applied a fourth order Butterworth filter and the cutoff period was empirically set at 50s. The integration on linear accelerations in Equation (1) amplified low-frequency drift of the accelerometers so high-pass filtering was needed (Fujitani 1981; Schulz et al. 2005; Edson et al. 1998; Miller et al. 2008). A proper cutoff was found at which the *u*, *v*, *w* variances and the covariance of horizontal (*u*) and vertical (*w*) wind speeds are not sensitive to the change of it. For horizontal accelerations the cutoff were 40s and for vertical acceleration was 80s (Miller et al. 2008).

2.2.2.3. TILT CORRECTION

Under ideal conditions, the measured mean vertical wind component $\overline{w}$ should be close to zero. However, if the sonic anemometer is tilted relative to the horizontal plane,

or if the wind stream is deflected by flow distortion (Yelland et al. 2002; Miller et al. 2008), the measured $\overline{w}$ may not be close to zero and would cause error in both momentum and scalar fluxes (Lee et al. 2005; Kaimal and Haugen 1969). Therefore, it is always necessary to monitor mean vertical velocity to track the effects of flow distortion and/or anemometer tile, and apply tilt correction to remove this measurment error

Following Miller et al. (2008), we applied a 'planar fit' method (Wilczak et al. 2001) to resolve the the tilt angles for the sonic anmometer and the motion sensor using a least square regression. The 20-min mean vertical wind component $\overline{w_1}$ is a function of 20-min mean horizontal wind speeds $\overline{u_1}$ and $\overline{v_1}$:

$$\overline{w_1} = b_0 + b_1\overline{u_1} + b_2\overline{v_1} \quad (18)$$

and the coefficients b_0, b_1, b_2 are determined by linear regression and used to obtain pitch (θ)and roll (ϕ) angles (Lee et al. 2005). The effect of offset between the motion sensor and anemometer on their respective tilt angles was accounted for following Miller et al. (2008).

2.2.2.4. Low-pass Filter Design

Considering the *CCGS Amundsen* is relatively large in size, flow distortion could be a big issue (Pedreros 2003; Fairall et al. 2003; Miller et al. 2010; O'Sullivan et al. 2013; Prytherch et al. 2015). To further eliminate noise at high frequencies, we applied a low-pass filter. As our sampling frequency is 10 Hz, we set the stop-band edge frequency at 5 Hz. The filter that meets our need should have maximum flatness in the pass band and a relatively wide transition band with an appropriate gradient. The desirable characteristics

of an IIR filter over an FIR filter is that an IIR filter has lower side-lobes in the stop-band than an FIR filter of the same order (Proakis and Monolakis 1996).

The IIR *Chebyshev* Type I was selected and tested. This specific kind of filter can minimize the absolute difference between the ideal and the actual frequency response over the entire pass-band and reach maximally flat for stop-band response. Comparing to a *Buttorworth* filter, the *Chebyshev* Type I filter has the advantage of a more rapid transition from pass-band to stop-band.

Filter design was realized with *Matlab*® Filter Design and Analysis (FDA) tool. The FDA tool offers user-specified pass-band and stop-band frequencies and attenuations and can automatically match the minimum order. The parameters that make a difference to the magnitude response are pass-band edge frequency F_{pass} and stop-band attenuation A_{stop}. The phase shift caused by applying IIR filter can be eliminated via the use of *filtfilt* function in Matlab. By trying out different combinations of F_{pass} and A_{stop}, the best performing filter was determined by visually comparing the mean slope with the theoretical model (Kaimal et al. 1972) and the overestimation before and after applying the filter. The frequency magnitude response of the filter applied is shown in **Figure 3.**

2.2.2.5. NOTCH FILTER DESIGN

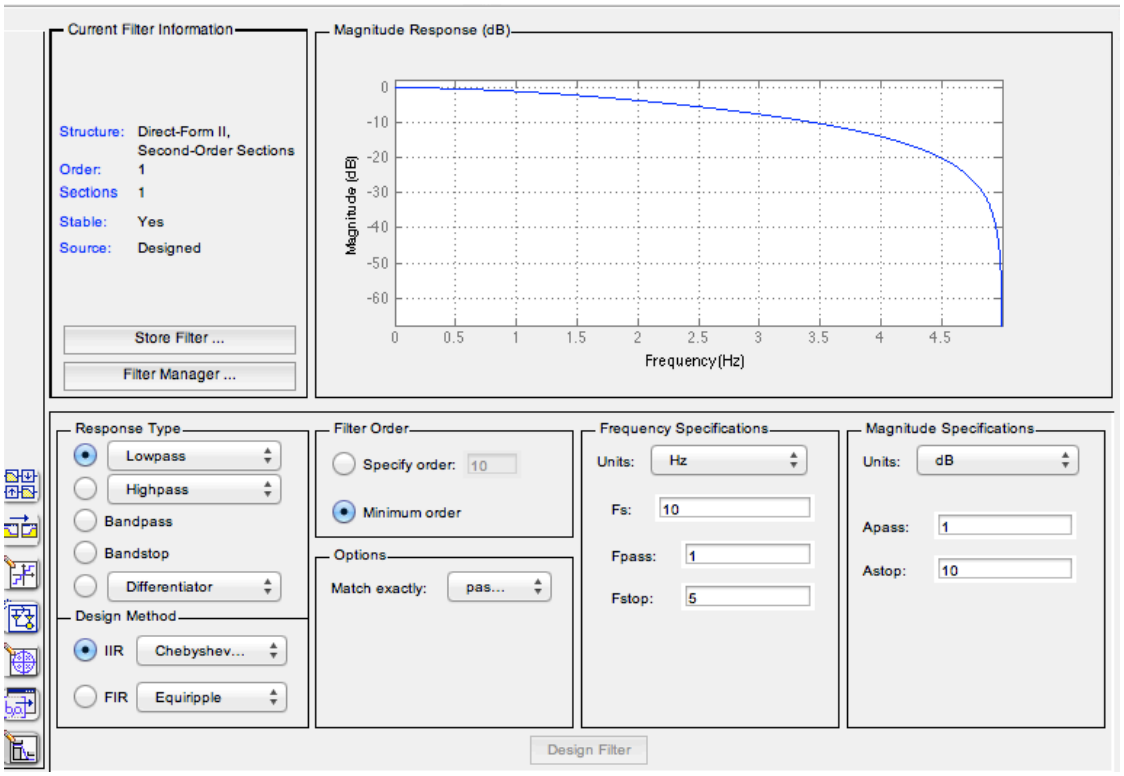

Figure 3. Low-pass filter parameters and magnitude response.

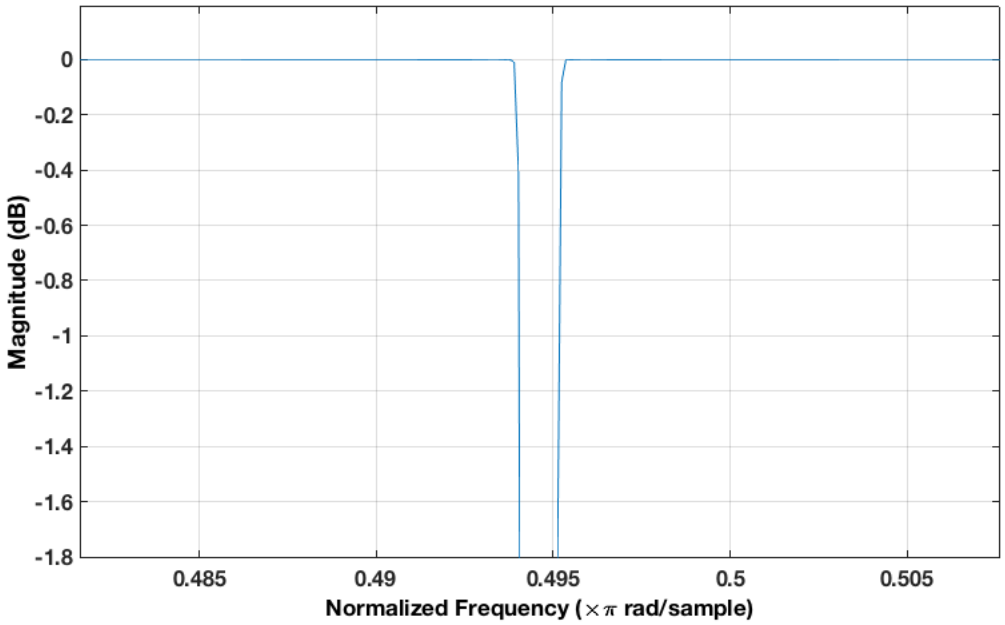

Figure 4. Notch filter magnitude response

The notch filter is a type of band-stop filter that can eliminate frequencies at a small specific range. Notch filters are in widely uses when certain frequency components need to be rejected, as for instance what might be required if imperfect motion correction. The notch filter was designed using *Matlab*® signal processing toolbox. Parameters controlling the characteristic of a notch filter involve filter order (N), centre frequency (F_0), quality factor (Q) and pass-band ripple (A_p). Higher orders ensure steeper slopes in its frequency response but are more complex and take more time for computing. On examining spectra and co-spectra, we decided to use the order of 10, which was deemed to retain proper co-spectra shape. As the main-lobe of the frequency to be eliminated occupies about 2 to 3 samples on average, a very narrow bandwidth was needed and Q was determined at 500. The centre frequency F_0 was found for each period by detecting the maximum over a small window over the power spectra. The frequency magnitude response of the notch filter is discussed in Section 3.2.1.3 and shown in **Figure 4**.

2.2.2.6. Other Corrections and Flux Calculation

After pre-processing for the platform effects described above, fluxes were calculated within each 20-minute interval using *EddyPro*®. Corrections and calculations accomplished in sequence by *EddyPro*® included angle of attack correction, coordinate rotation, time lag compensation, density conversion, flux calculation, SND correction and spectral corrections (**Table 3**). Axis rotation was fulfilled by sector-wise planar fit method (Wilczak et al. 2001). The plane was equally divided into 12 sectors and rotation matrix was calculated for each 30-degree wind sector and applied to wind vector.

Compensation for time lag was accomplished with the embedded "covariance maximization with default" method (Fan et al. 1990). Minimum, maximum and a nominal times lag were set and when the time lag obtained by the covariance maximization method is out of range, the preset nominal time lag was used. The *LI-7000* at the heart of the closed-path system used in this study is able to output CO_2 and H_2O dry mole fraction simultaneously and easily converted to mixing ratio (Ibrom et al. 2007; Burba et al. 2012). Once the previously discussed procedures had been fulfilled, spectra and co-spectra were calculated (Stull 1988). For sensible heat flux, one extra correction was offered to transform sonic or acoustic temperature to actual air temperature for the SND correction (Schotanus et al. 1983; Aubinet et al. 2012). *EddyPro*® also provides low-pass filtering correction as well as high-pass filtering correction. For low-pass filtering correction, we chose to apply the fully analytic correction after Moncrieff et al. (1997). With this method, a series of transfer functions were defined and applied to the calculated co-spectra to compensate for high frequency loss (Moncrieff et al. 1997). For high-pass filtering corrections, *EddyPro*® offers correction following Moncrieff et al. (2004) (Lee et al. 2005). Analogous to low-pass filtering correction, high-pass spectral correction factor takes account for wind speed and atmospheric conditions and is run-to-run based.

3. RESULTS

3.1. DATA SCREENING

After the initial processing and motion correction of the EC data, we ended up with 1687 20-min runs. These runs were sent to *EddyPro*® for further processing and flux

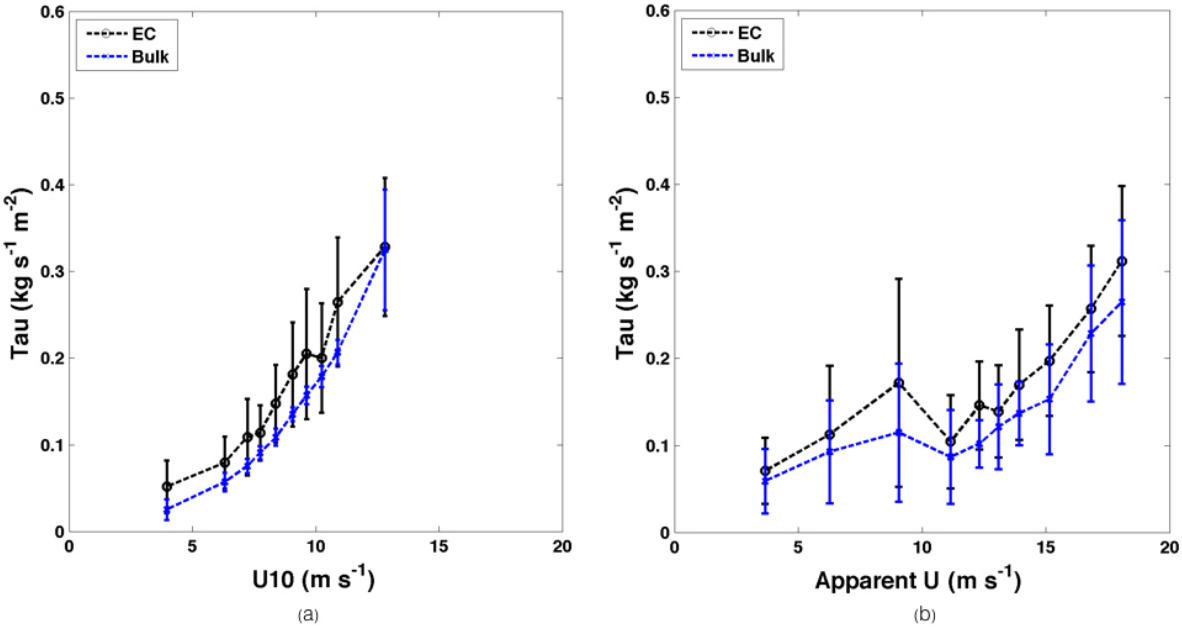

Figure 5. Momentum flux derived from the EC (black) and bulk method (blue) for open water condition shown as a function of U10 and apparent wind speed. Data is restricted to U10 greater than 2 m/s.

calculation. The resulting fluxes were subjected to additionally screening to remove fluxes calculated under less than ideal conditions that could not support the acquisition of good flux data. Fluxes could be biased under conditions of extremely high and low wind speeds; the former giving rise to sea spray on flux sensor and vibrations of the anemometer support arm, whereas under light winds it is likely the surface is decoupled from the measurement height because of insufficient turbulent mixing. Additionally relative wind direction and wind speed cold impact fluxes through the effect of flow distortion. A first step was to screen out periods whose spectral plots grossly deviated from shape predicted by theory. High EC momentum flux and associated scatter for wind for U10 less than 2 m/s suggest the EC system is unstable for these low winds. With

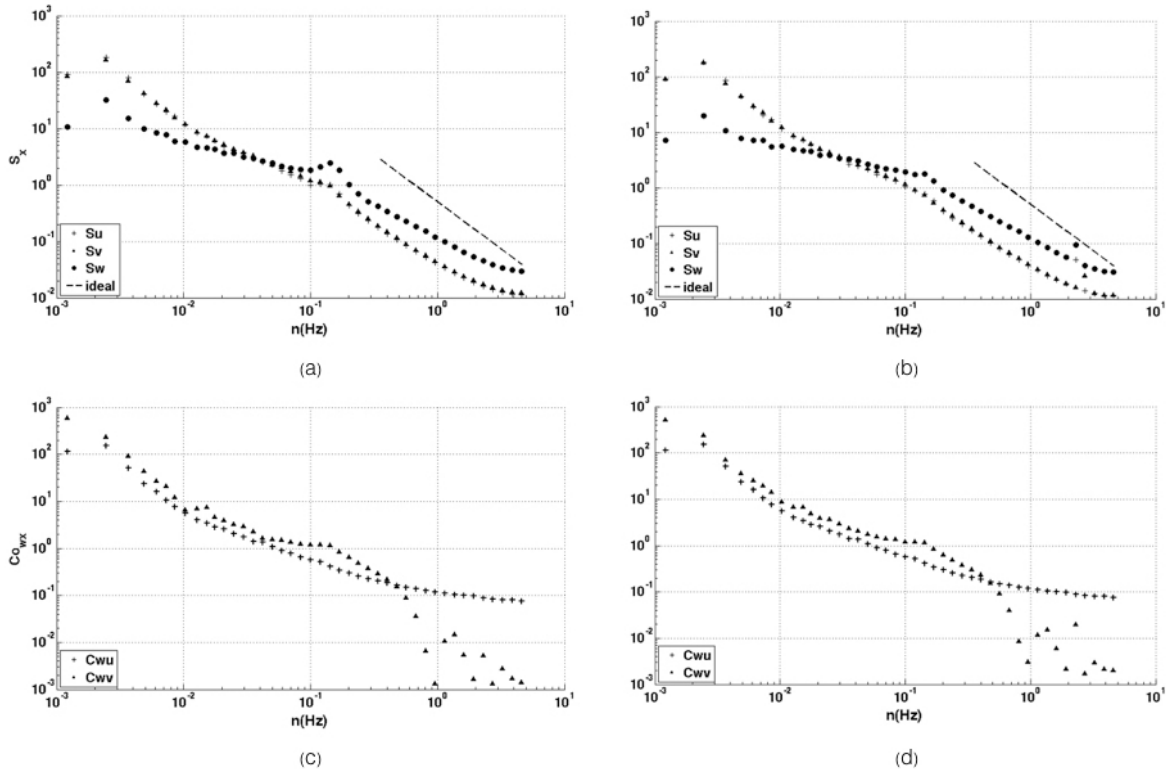

Figure 6. The ensemble-averaged spectra and co-spectra for measured (left) and motion corrected (right) wind velocities.

small wind removed from the data set, we realized that a period with which the average apparent wind speed is extremely high is also skeptical. As indicated in **Figure 5**, larger discrepancy and standard deviation occur when the apparent wind speed exceeds 14 m/s and thus need to be rejected. Spikes in EC results are not uncommon and associated with violations in EC assumptions and/or environmentally induced bias (e.g., frost or spray on sensors) and then outliers with unreasonably large fluxes were identified and removed. Periods with missing data in motion correction and flux calculation were also eliminated.

3.2. CO-SPECTRA AND EC FLUX

3.2.1. *Motion Correction Evaluation and Momentum flux*

3.2.1.1. Ensemble Averaged Spectra and Cospectra

The ensemble-averaged spectra and co-spectra for measured and motion corrected wind velocities (*w, u, v*) are shown against natural frequency in **Figure 6**. Motion peaks at around 0.18 Hz are seen in the spectra for all three motion channels and is most obvious in *w* (**Figure 6**(a)) and lead to the bump in *wu* co-spectra (**Figure 6**(c)). **Figure 6**(b)(d) are the post-motion corrected spectra and co-spectra and illustrate that motion is mitigated but not totally eliminated. Also noticeable is the noise picked up by the motion correction at about 2.5 Hz.

3.2.1.2. Angle of Attack

To explore the presence of wind-related bias on the motion correction, angle of attack was examined against relative wind directions. The distribution of relative wind directions to the bow of the ship (**Figure 7**) indicates that was most often ± 30° from the bow (considered 0° or 360°). The mean and standard deviation of angle of attack are shown in degrees as a function of relative wind direction for uncorrected and motion and tilt corrected wind in **Figure 8**. The average AoA for uncorrected wind is around 7 degrees and AoA was generally reduced for all wind direction after motion and tilt correction but could still reach 5 degree for bow-on wind. The correction does bring AOA on average closer to zero. However, our motion correction appears to have exasperated the relationship for winds flowing over the bow of the ship. The standard deviation decreased only for port-side (negative degrees) winds but was significantly amplified for winds off the bow and slightly amplified for starboard-side (positive degrees) winds (**Table 4**).

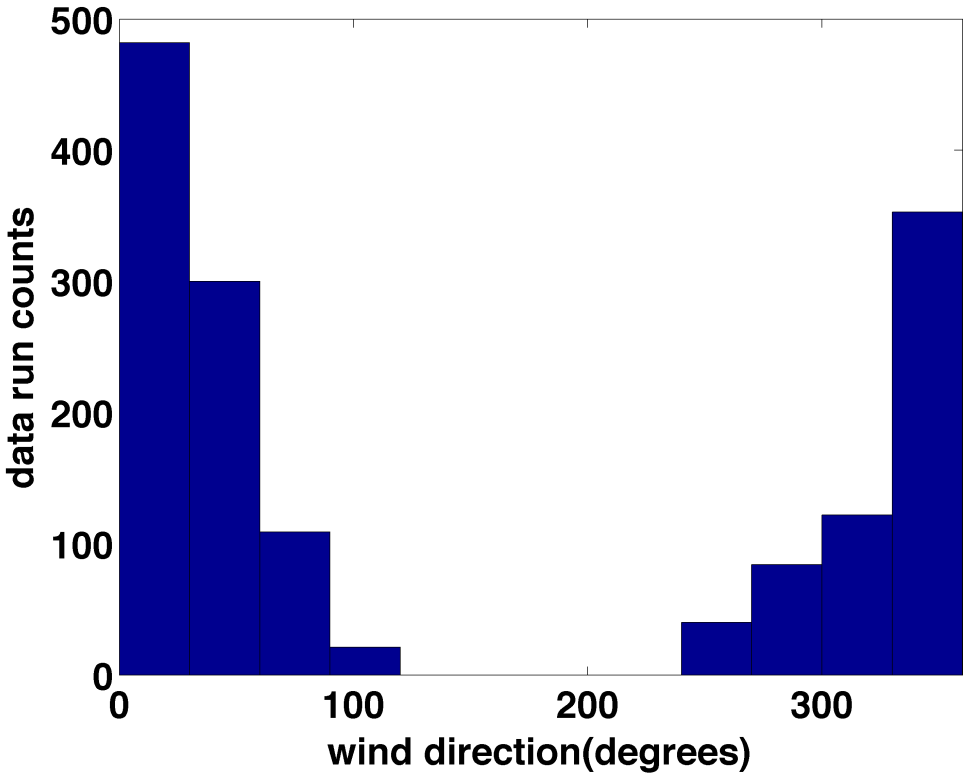

Figure 7. Histogram of relative wind directions for all 20-min runs.

The operating envelope for *Wind-Master Pro* (Gill Instruments) suggested by the manufacturer is ±20° (Nakai and Shimoyama 2012; Cava et al. 2008; Nakai et al. 2006; Gash and Dolman 2003). 20-minute runs with angle of attack greater than 20 degrees were excluded in accord with the manufacturer's suggestion.

3.2.1.3. WU CO-SPECTRA AND MOMENTUM FLUX

The ensemble average for the covariance-normalized *wu* co-spectra are plotted against normalized frequency for port-side (±45° relative to port), over the bow (±45° relative to bow) and starboard-side (±45° relative to starboard) relative wind directions

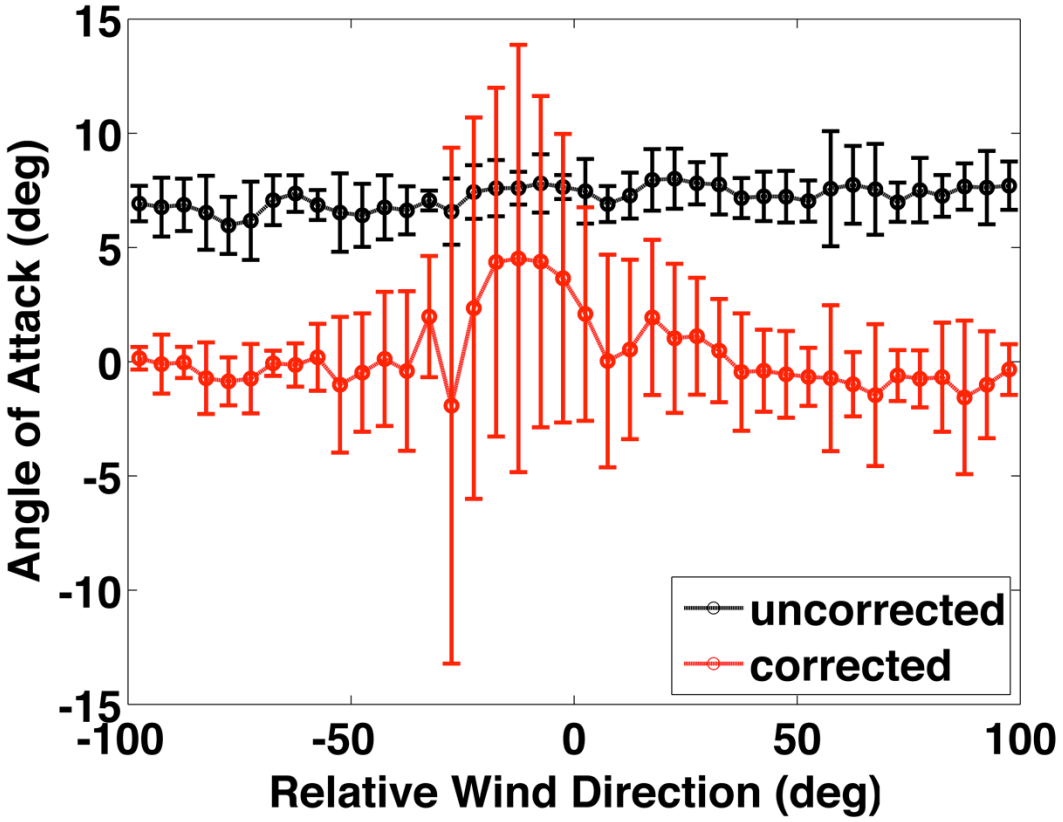

Figure 8. The angle of attack (AoA) plotted against relative wind direction relative to the bow for uncorrected and corrected wind. Negative degrees represent port-side and positive degrees represent starboard-side.

for apparent wind speed classes: low (0-4 m/s); mid-low (4-8 m/s), mid-high (8-12 m/s) and high winds, along with Kaimal et al's (1972) theoretical curves in **Figure 9.**

By comparing to Kaimal's model, for apparent wind smaller than 4 m/s, excessive momentum flux at all frequencies are seen for both portside-side and off-the-bow winds (**Figure 9** (a) (b)). As the wind develops, the overestimation seems to be decreased to a great extent for all wind directions (**Figure 9**). This is not unexpected as the momentum flux is more strongly impacted by flow distortion relative to the scalar fluxes (Pedreros

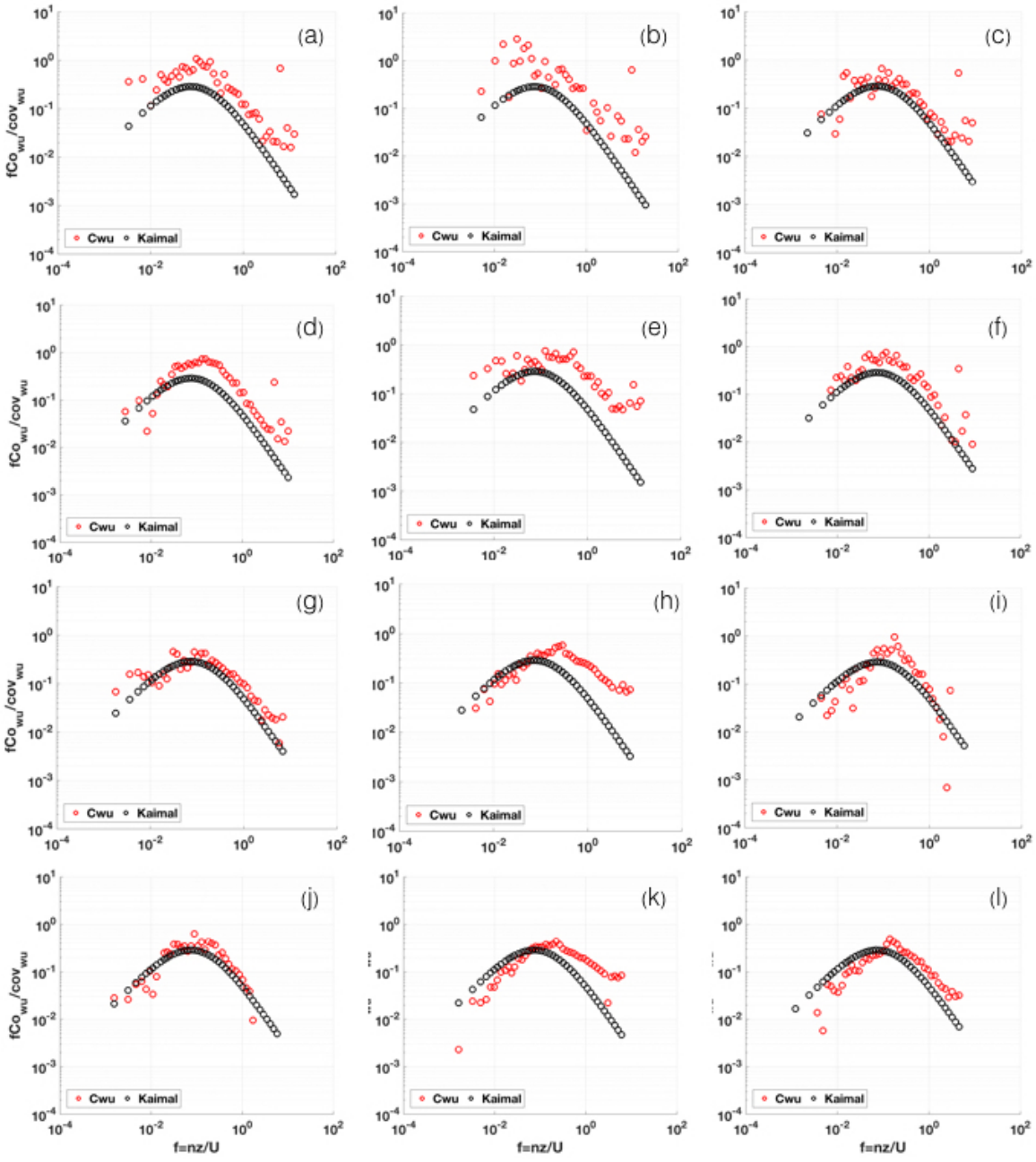

Figure 9. Shown in red circles are the ensemble-averaged co-spectra of horizontal (u) and vertical wind component (w) for relative wind direction within ± 45° of the port (left), ± 45° of the bow (middle) and ± 45° of the starboard (right) for different apparent wind speed classes. Apparent wind speed are classed into four levels: low (0 – 4 m/s), mid-low (4 – 8 m/s), mid-high (8 – 12 m/s) and high (> 12 m/s), shown

as the four rows of figures. Shown in black circles are the theoretical curves (Kaimal et al. 1972). The area under the curve is proportional to the momentum flux. (a) low winds from the port side; (b) low winds from the centre; (c) mid-low winds from the port side; (d) mid-low winds from the port side; (e) mid-low winds from the starboard side; (f) mid-high winds from the port side; (g) mid-high winds from the centre; (h) mid-high winds from the starboard side; (i) high winds from the centre; (j) high winds from the starboard side.

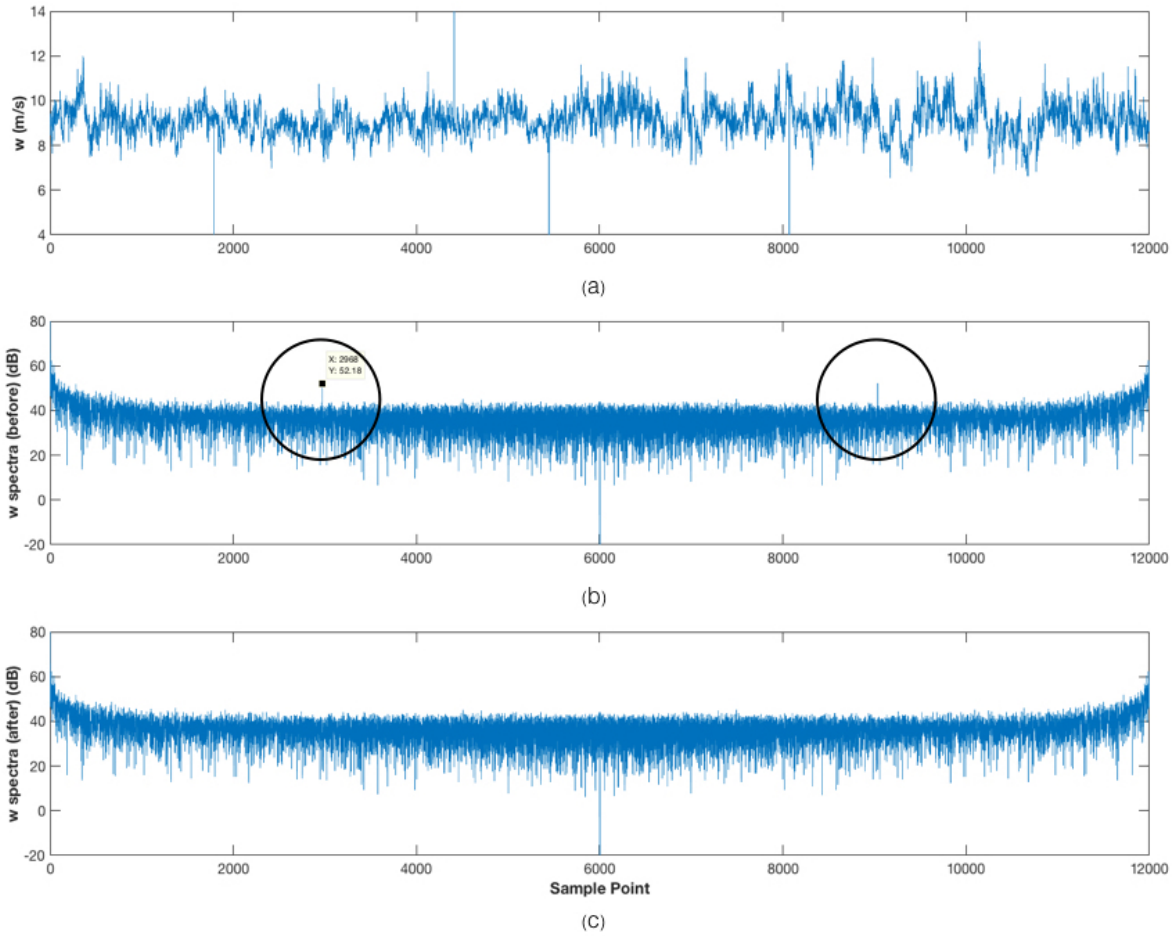

Figure 10. (a) Time series of a sample 20-min period; (b) The power spectra of the 20-min period; the black circled are the noise to be eliminated; (c) The filtered power spectra.

Table 4. Mean and standard deviation of angle of attack for different wind direction

		Port	**Bow**	**Starboard**
Uncorrected	Mean	6.74	7.54	7.51
	Std	1.25	1.15	1.46
Corrected	Mean	-0.26	2.13	-0.99
	Std	1.09	6.18	2.27

Table 5. The percentage of momentum flux overestimation compared to Kaimal's curve for different wind speed classes and wind directions before and after the Notch filter was applied.

	Port pre-filered	Notched	**Bow** pre-filtered	Notched	**Stbd** pre-filtered	Notched
Low (0<U10<4 m/s)	1292	851	809	589		
Low (2<U10<4 m/s)	1292	851	527	348		
Low (0-4 m/s)	569	266	775	366	310	142
Mid-low (4-8 m/s)	288	205	398	530	240	99
Mid-high (8-12 m/s)	70	69	354	367	52	18
High (>12 m/s)	-30	-21	255	260	91	88
Ensemble (u10>2-AprtU<U14)	241	153	306	308	136	93

2003). Comparing vertically between the three directions, off-the-bow wind (**Figure 9** (b) (e) (h) (k)) separates from side winds at frequencies greater than 0.1 Hz. Port-side moderate high winds (**Figure 9**(g)) performs the best among the three, with its co-spectra agreeing well with Kaimal's model. The starboard-side *wu* co-spectra seem to lose normalized co-spectra at frequencies beyond 1 Hz for wind class 4-8 m/s (**Figure 9**(i)).

Noise was found in the *wu* co-spectra at natural frequency of about 2.47 Hz. The notch filter previously introduced in **Section 2.2.2.5** was used and **Figure 10** reveals the FFT of a sample time series before and after the notch filter was applied. It appears the noise was removed. The effect of the Notch filter is also reflected in the ensemble averaged wu co-spectra for low wind (**Figure 11**). Percent of the overestimation of the area under the theoretical curve pre- and post- notch filter for wind speeds and wind directions classes is presented in **Table 5**. High EC momentum flux and associated scatter for wind for U10 less than 2 m/s suggest the EC system is unstable for these low winds.

The *Chebyshev* low pass filter dealt with a broader range of frequencies and the post-filtered *wu* co-spectra for the three relative wind direction class illustrate the low-pass filter with the same parameters seems to work best for off-the-starboard winds (**Figure 12** (f)) whereas the port-side wind is shown to be overcorrected (**Figure 12**(d)) and the off-the-bow wind not conforming to the same corrected pattern (**Figure 12**(e)). Percent of the overestimation of the area under the theoretical curve pre- and post- *Chebyshev* filter for the three relative wind direction classes is presented in **Table 6**.

3.2.2. *SCALAR CO-SPECTRA*

The *wT* co-spectra for all directions of relative wind (**Figure 13**) follow the theoretical curves of Kaimal et al. (1972). The ensemble averaged *wT* co-spectra for all screened periods illustrate the fairly good bell shape but has noise over all frequencies for off-the-port wind (**Figure 13**(a)) and noise at mid and high frequency for over-the-bow

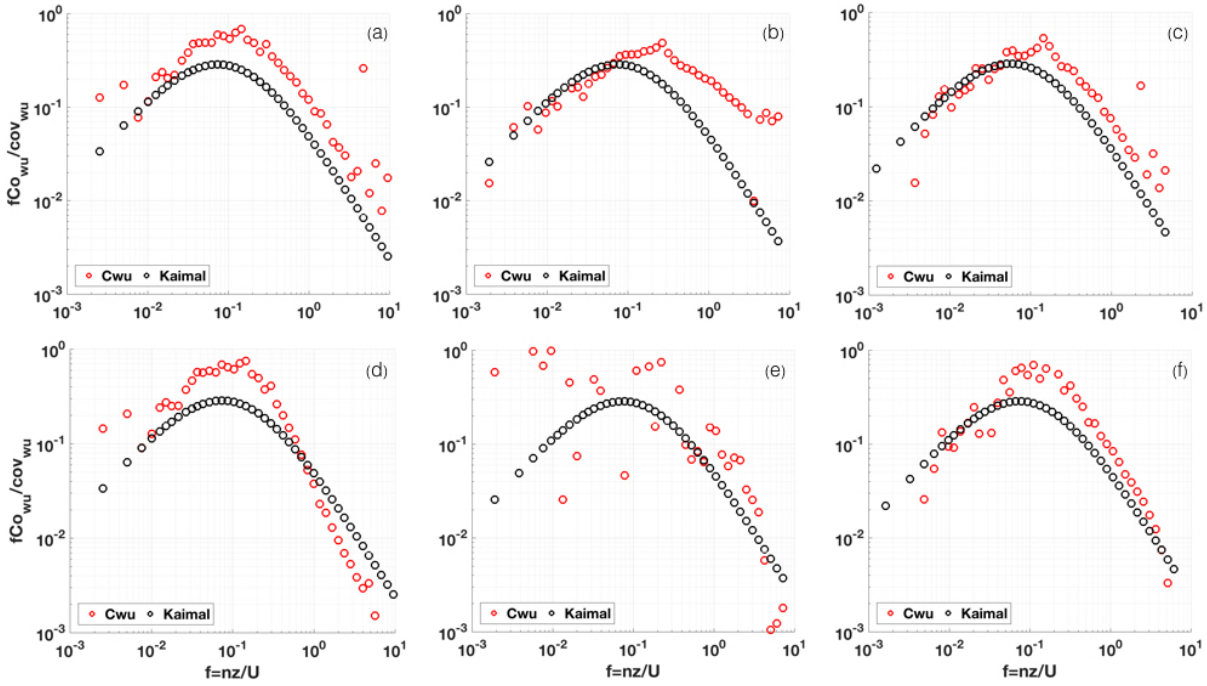

Figure 12. Shown in red circles are the ensemble-averaged co-spectra of horizontal (*u*) and vertical wind component (*w*) for screened periods. Shown in black circles are the theoretical curves (Kaimal et al., 1972). The area under the curve is proportional to the momentum flux.

wind (**Figure 13**(b)). Starboard-side *wT* co-spectra show very close agreement with the theoretical curve with slight overestimation over frequencies at low and high ends (**Figure 13**(c)). As expected, the *wT* co-spectra for all relative wind directions seem to correspond to their *wu* co-spectra.

The wCO_2 co-spectra (**Figure 14**) only weakly conform to the theoretical curves relative to the *wu* and *wT* co-spectra. In the ensemble for all screened periods, we see a diminished high frequency signal and hypothesize that the high frequency CO_2 fluctuations have been dampened by the intake tube. A peak is seen at normalized frequency of around 0.3 in all co-spectra. This peak may be explained as the remaining

motion noise. **Figure 14**(b) also indicates flux attenuated at the normalized frequency range of 0.01 to 0.2 for winds coming over the bow. Percent of the overestimation of the area under the theoretical curve for wT and wCO_2 co-spectra is presented in **Table 7**.

3.3. METEOROLOGY AND SEA ICE CONCENTRATION

The sea ice concentration is shown in **Figure 15** based on science log. The four classes are open water, low ice concentration (1/10 – 3/10), medium ice concentration (4/10 – 6/10) and high ice concentration (7/10 – 10/10). For much of the cruise the ship experienced either no ice, or low ice cover. Pockets of high ice were encountered within the passages of the Arctic Archipelago, northeast Baffin Bay and northwest of Banks Island in the Beaufort Sea. The largest stretch of open water was observed in the southern Beaufort Sea and in Amundsen Gulf.

Table 6. The percentage of momentum flux overestimation compared to Kaimal's curve for different wind speed classes and wind directions before and after the low-pass filter was applied.

	Port		**Bow**		**Stbd**	
	pre-filtered	Low-pass filtered	pre-filtered	Low-pass filtered	pre-filtered	Low-pass filtered
Overestimation	241	31	306	-197	136	97

Table 7. The percentage of sensible flux and CO_2 flux overestimation compared to Kaimal's curve for different wind direction classes.

	Port	Bow	Stbd
H	241	169	73
CO_2	70	45	-8

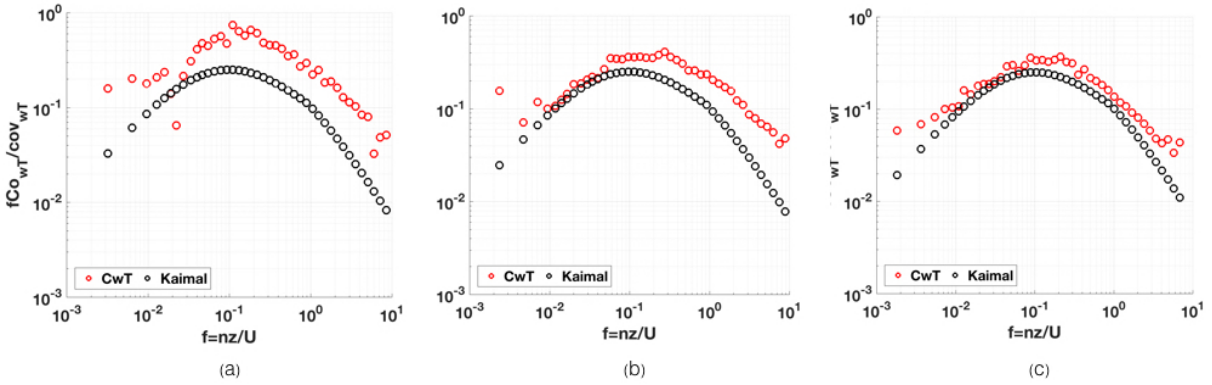

Figure 13. Shown in red circles are the ensemble-averaged co-spectra of temperature (*T*) and vertical wind component (*w*) for screened periods. Shown in black circles are the theoretical curves (Kaimal et al., 1972). The area under the curve is proportional to the sensible heat flux.

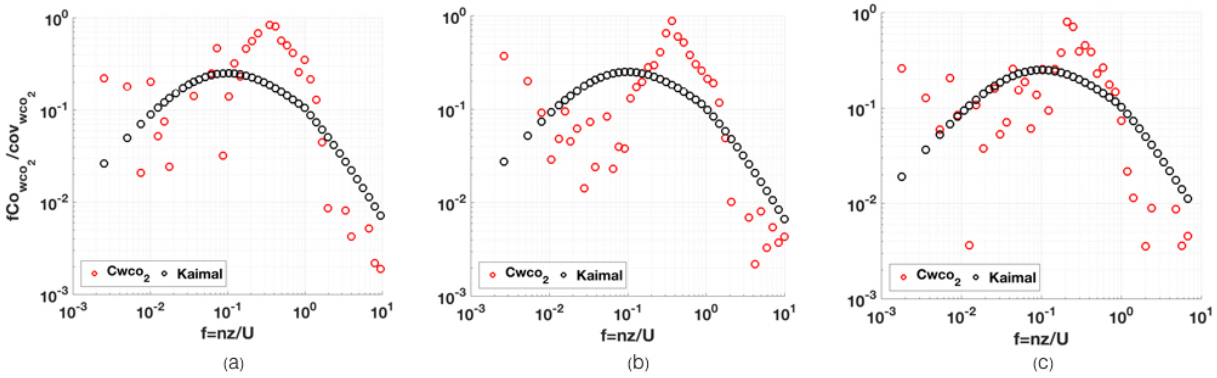

Figure 14. Shown in red circles are the ensemble-averaged co-spectra of CO_2 and vertical wind component (*w*) for wind from the port side (left), centre (middle) and starboard side (right) of the bow. Shown in black circles are the theoretical curves (Kaimal et al., 1972). The area under the curve is proportional to the CO_2 flux.

Over the cruise the ship experienced periods of high winds (**Figure 16**), with apparent speeds approaching 20 m/s. True wind scaled to 10 m never exceeded 15 m/s, and more often ranged between 5 and 10 m/s.

Air temperature ranged from ~ 22°C to -10°C over the cruise (**Figure 17**), and averaged 4.29 °C. Shown also in the figure is the sea (or sea ice) surface temperature (SST). As expected SST generally tracked air temperature, particularly after the first month of the experiment.

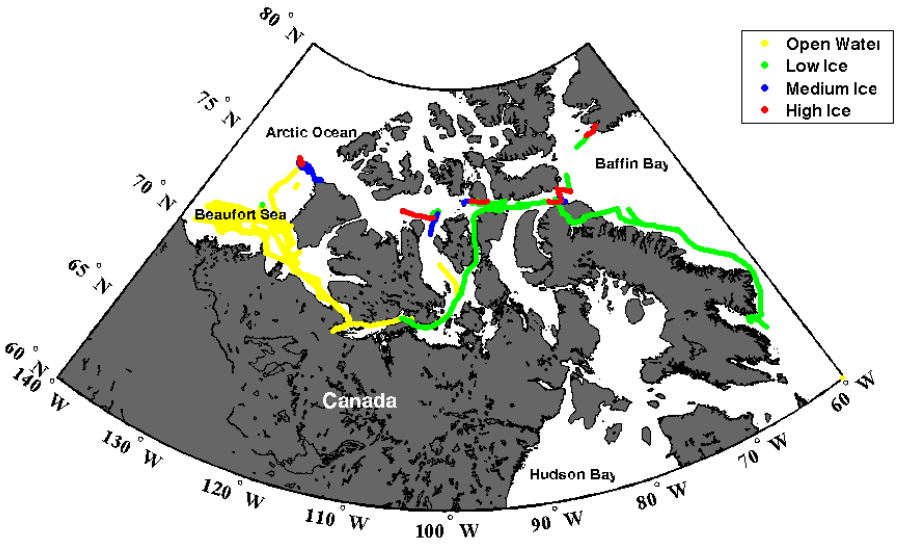

Figure 15. Sea ice concentration on map. The four classes are based on science log recorded on a scale of 10. Open water (yellow): 0/10 sea ice concentration, low ice (green): 1/10 to 3/10 concentration, medium ice (blue): 4/10 to 6/10 and high ice (red): 7/10 to 10/10.

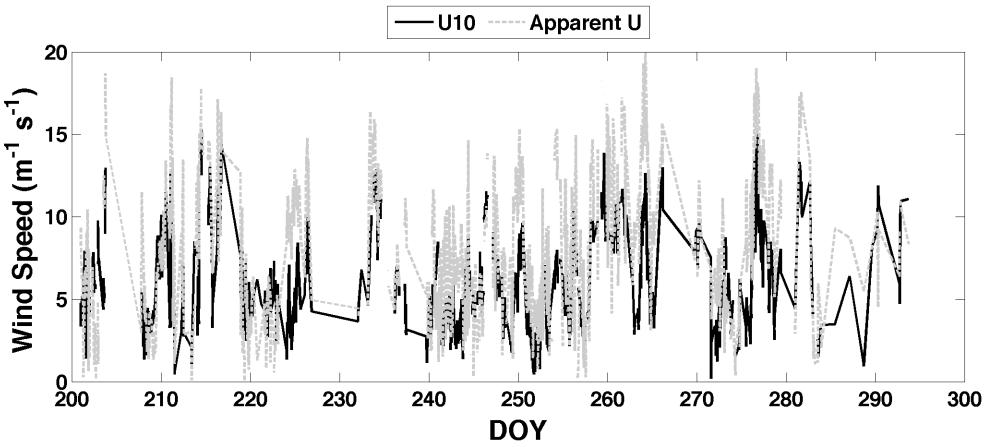

Figure 16. Time series for U10 and apparent wind during the entire cruise (Day 201 to Day 293).

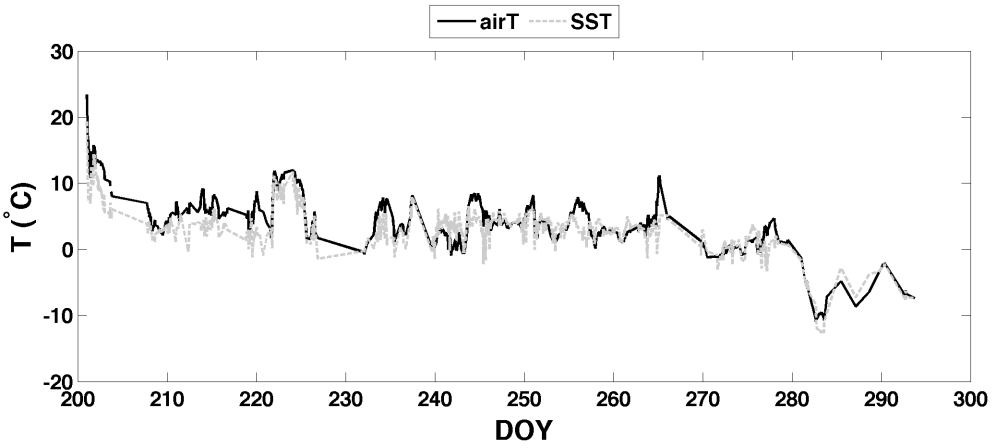

Figure 17. Time series for air temperature (airT) and sea surface temperature (SST) during the entire cruise (Day 201 to Day 293).

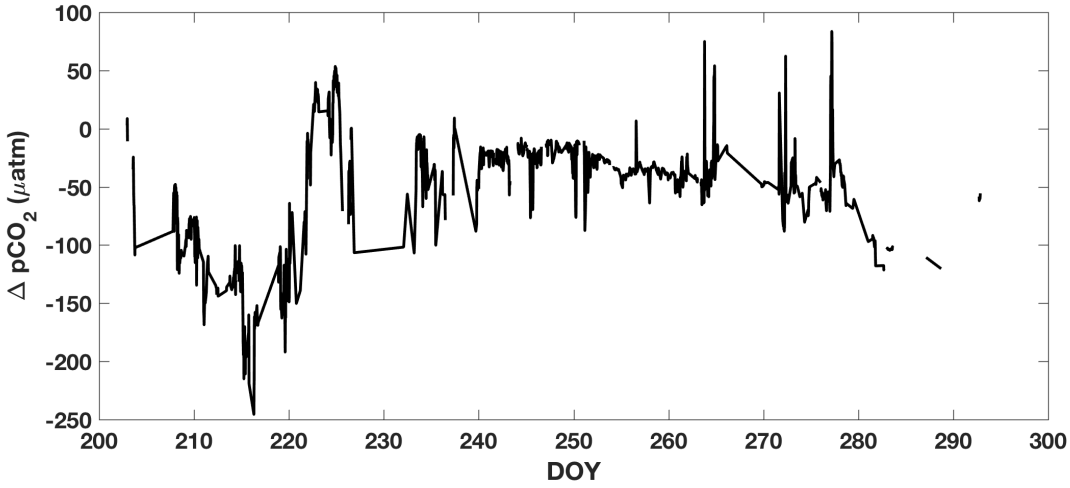

Figure 18. Time series for ΔpCO_2 over the entire cruise (Day 201 to Day 293).

3.4. MOMENTUM, HEAT AND CO_2 FLUXES

The time series of the difference in CO_2 partial pressure between the sea surface and air (ΔpCO_2 appears in **Figure 18**). Evident in the figure are periods of pronounced under pCO_2 under-saturation in the seawater relative to the atmosphere (e.g., strongly negative ΔpCO_2 between day of year 210 and 220) and over-saturation (e.g. strongly positive ΔpCO_2 between day of year 220 and 230). Over much of the cruise however the ΔpCO_2 only shows modest pCO_2 under- or over-saturation. With few exceptions ΔpCO_2 is within 50 μatm of zero between day of year 230 and 280.

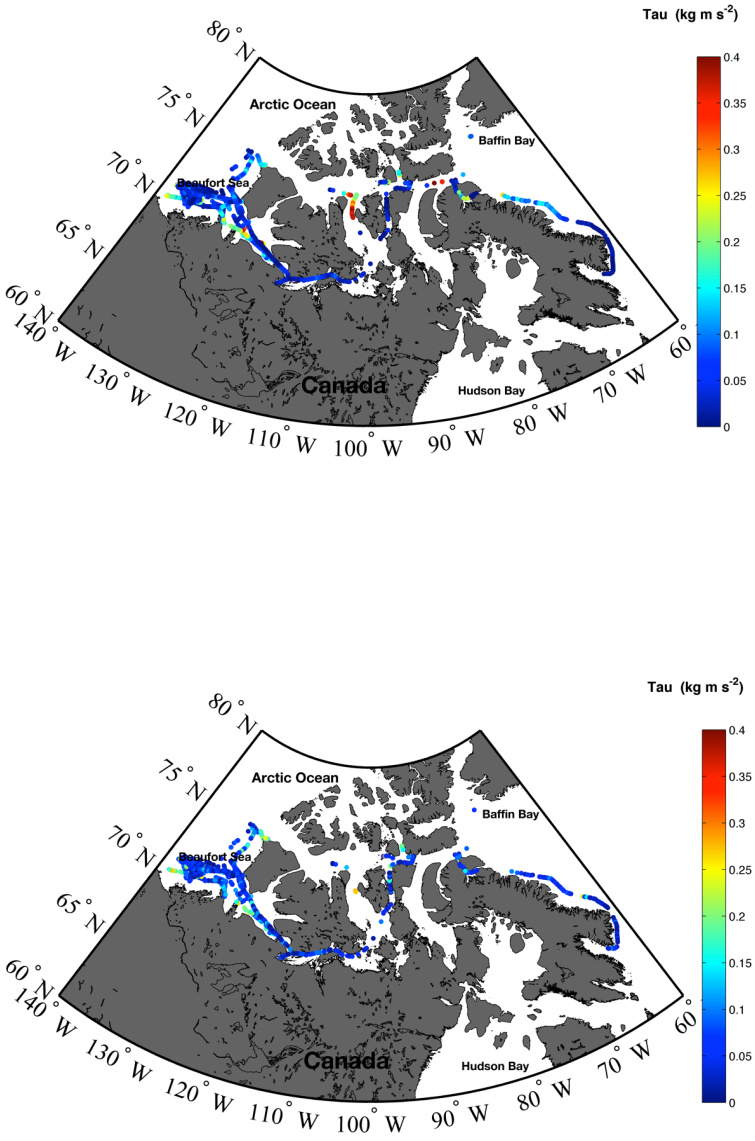

Figure 19. Momentum fluxes visualized on maps using bulk parameterization (COARE 3.0) (top) and the EC approach (bottom).

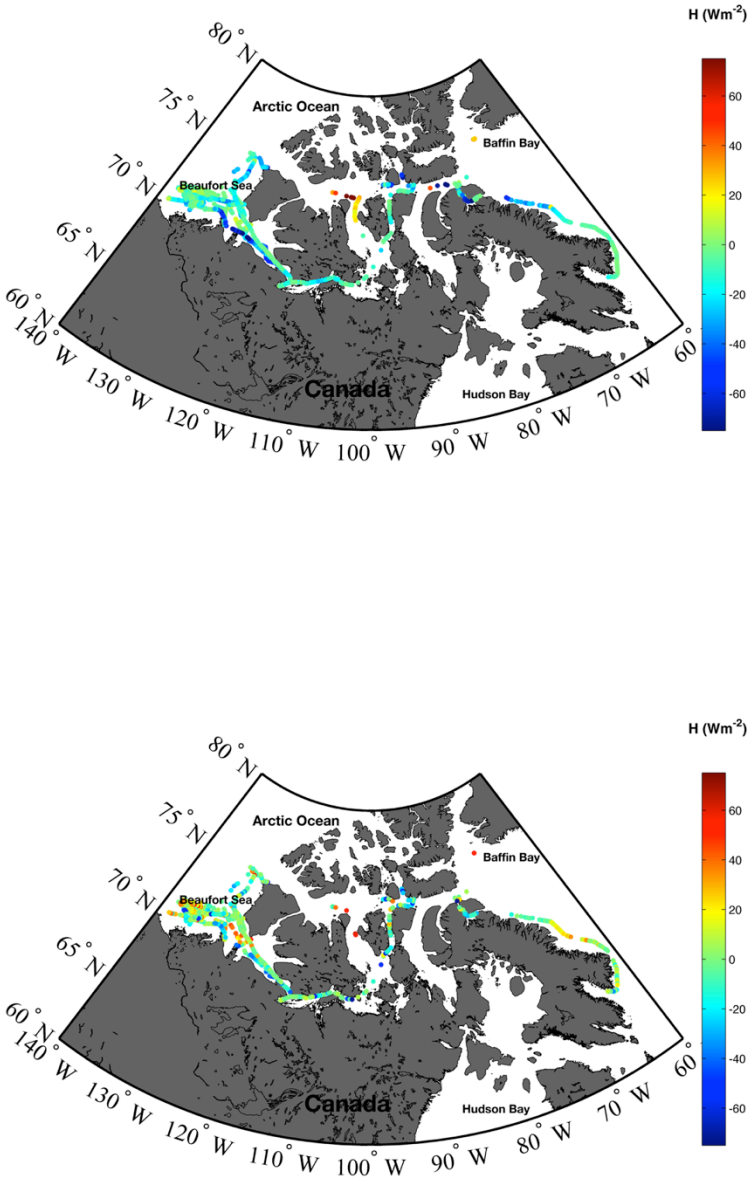

Figure 20. Sensible heat fluxes visualized on maps using bulk parameterization (COARE 3.0) (top) and the EC approach (bottom).

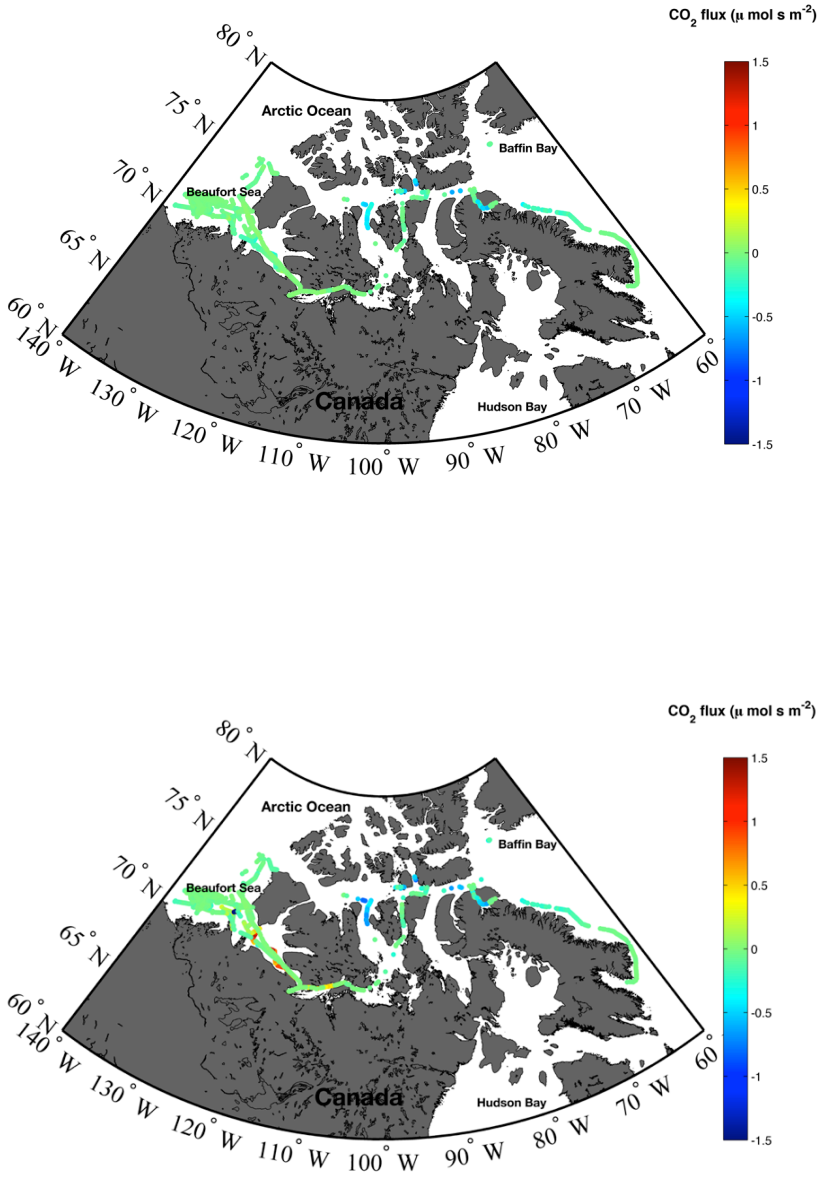

Figure 21. CO_2 fluxes visualized on maps using bulk parameterization (COARE 3.0) (top) and the EC approach (bottom).

Illustrated in **Figure 19** (b), **Figure 20** (b) and **Figure 21** (b) are maps where the momentum, sensible heat and CO_2 fluxes are visualized for the bulk and EC solution to the fluxes respectively. High momentum flux is attributed to strong winds that were encountered off the west coast of Prince of Wales Island, in Amundsen Gulf, in the southeastern Beaufort Sea and at the northwestern tip of Banks Island.

Negative sensible heat fluxes (indicating heat loss by the atmosphere) are extensively observed in the south of Beaufort Sea while returning from Beaufort Sea and through Kugluktuk. Pronounced heat loss by the atmosphere is also seen off the coast near Resolute. Positive fluxes took place in Amundsen Gulf, the middle of Beaufort Sea and north and southeast of Stefansson Island.

The CO_2 fluxes over a large fraction of the measuring periods are in the range of -0.5 to 0.5 $\mu mol\ m^{-2}\ s^{-1}$. There seems to be relatively large CO_2 outgassing to the north of Baffin Bay and in the south of Beaufort Sea. CO_2 absorption occurred in the middle of Beaufort Sea and near Resolute.

3.5. COMPARISON OF EC AND BULK FLUXES

Momentum, heat and CO_2 fluxes as derived using EC and the bulk approach are shown on the same axes in **Figures 22** to **25**, while statistics describing the relationship are provided in **Table 8**. The fluxes are compared graphically in **Figure 26**.

In open water environment, on some particular days (Day 245, Day 250 Day 279), the EC flux is double the amplitude of bulk momentum flux (**Figure 22**. The apparent wind speeds for these days are excessively high (~15 m/s) (**Figure 16**). In general the

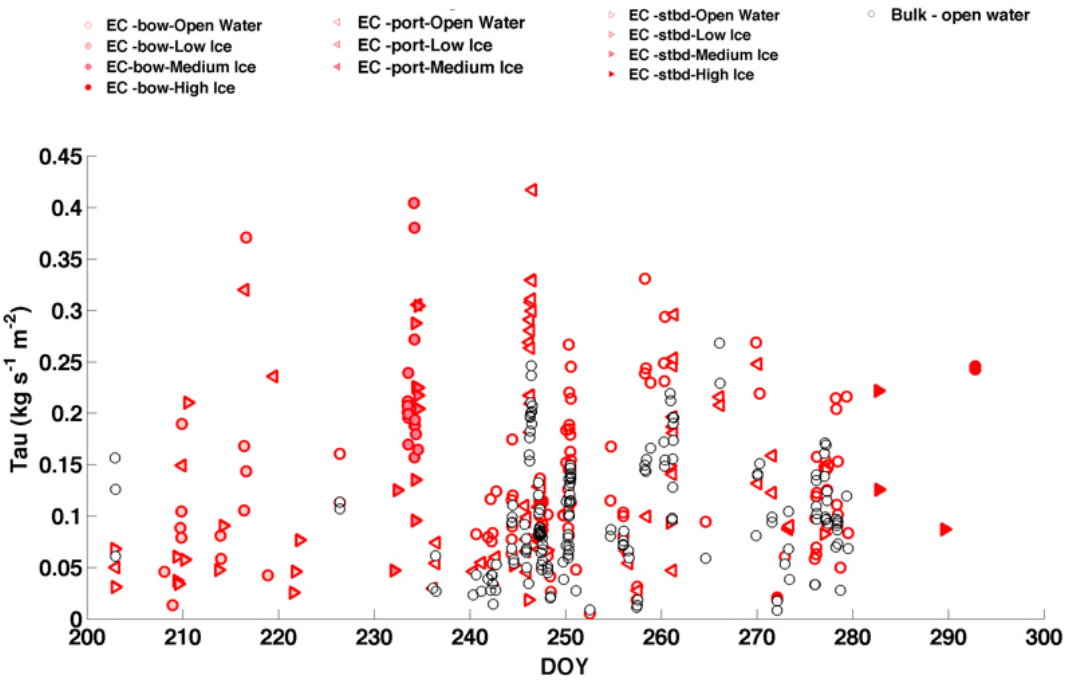

Figure 22. Scatter plots of each screened 20-minute period for EC (black) and bulk (red) momentum flux over the duration of the cruise. Circles denote wind coming off the bow, left triangles represent wind come from the portside and right triangles represent wind coming from the starboard side. Sea ice concentration is indicated by the color. The darker, the higher ice concentration.

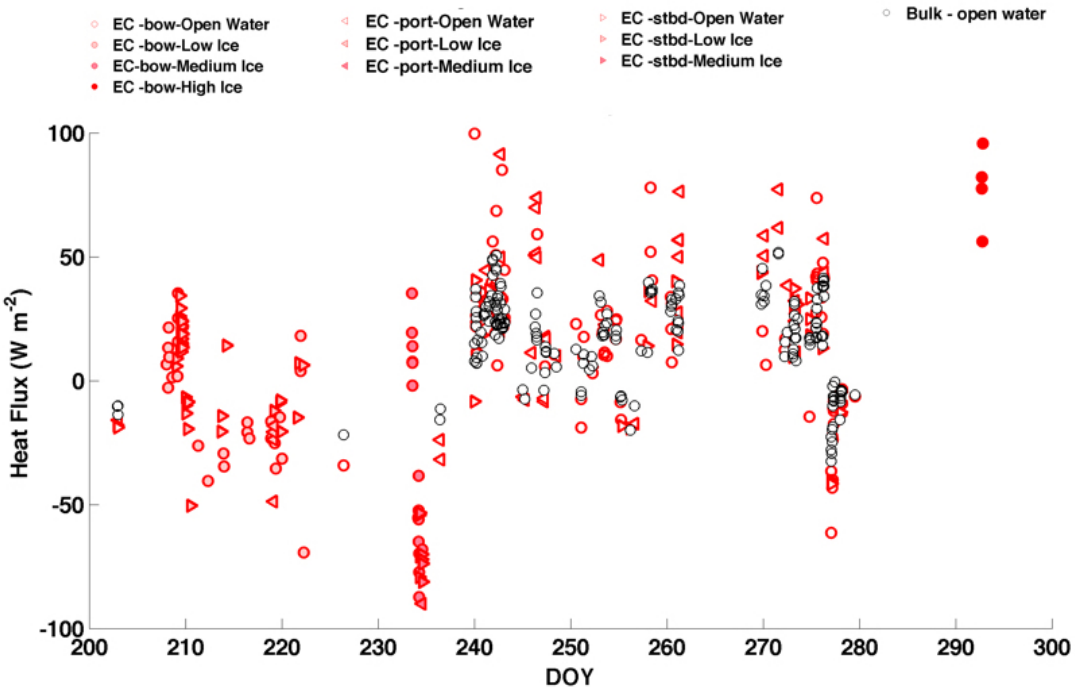

Figure 23. Scatter plots of each screened 20-minute period for EC (black) and bulk (red) sensible heat flux over the duration of the cruise. Circles denote wind coming off the bow, left triangles represent wind come from the portside and right triangles represent wind coming from the starboard side. Sea ice concentration is indicated by the color. The darker, the higher ice concentration.

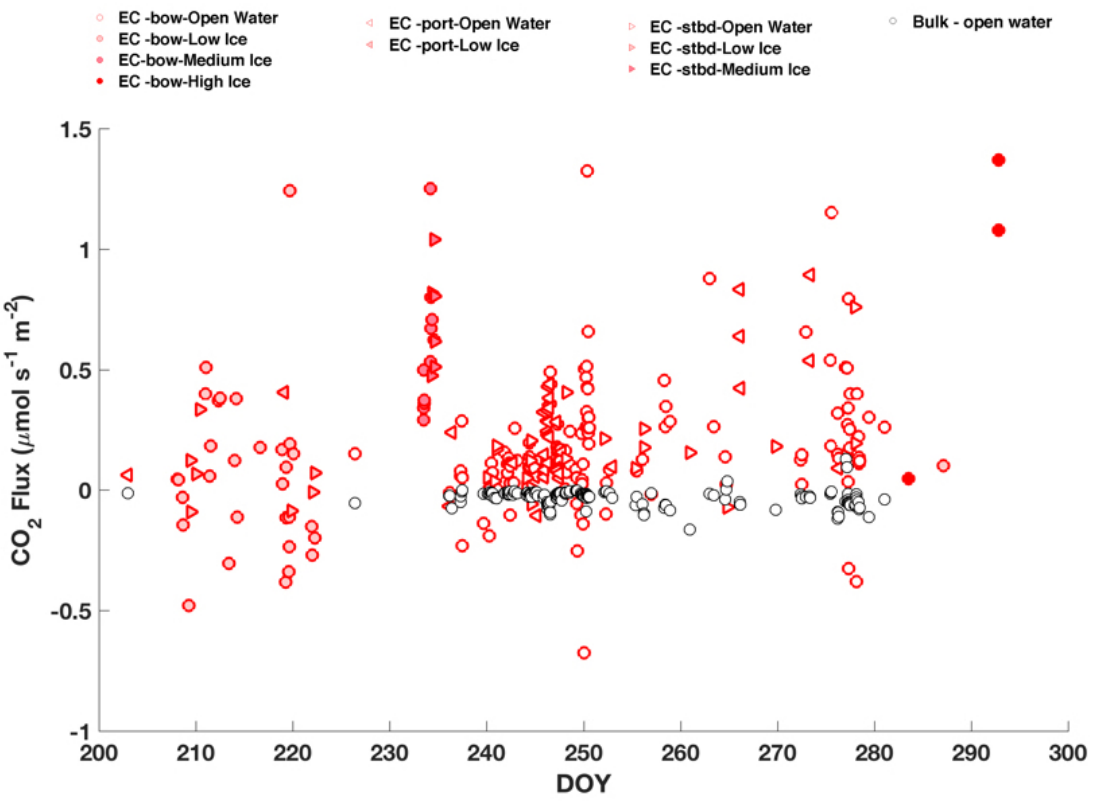

Figure 24. Scatter plots of each screened 20-minute period for EC (black) and bulk (red) CO_2 flux over the duration of the cruise. Circles denote wind coming off the bow, left triangles represent wind come from the portside and right triangles represent wind coming from the starboard side. Sea ice concentration is indicated by the color. The darker, the higher ice concentration.

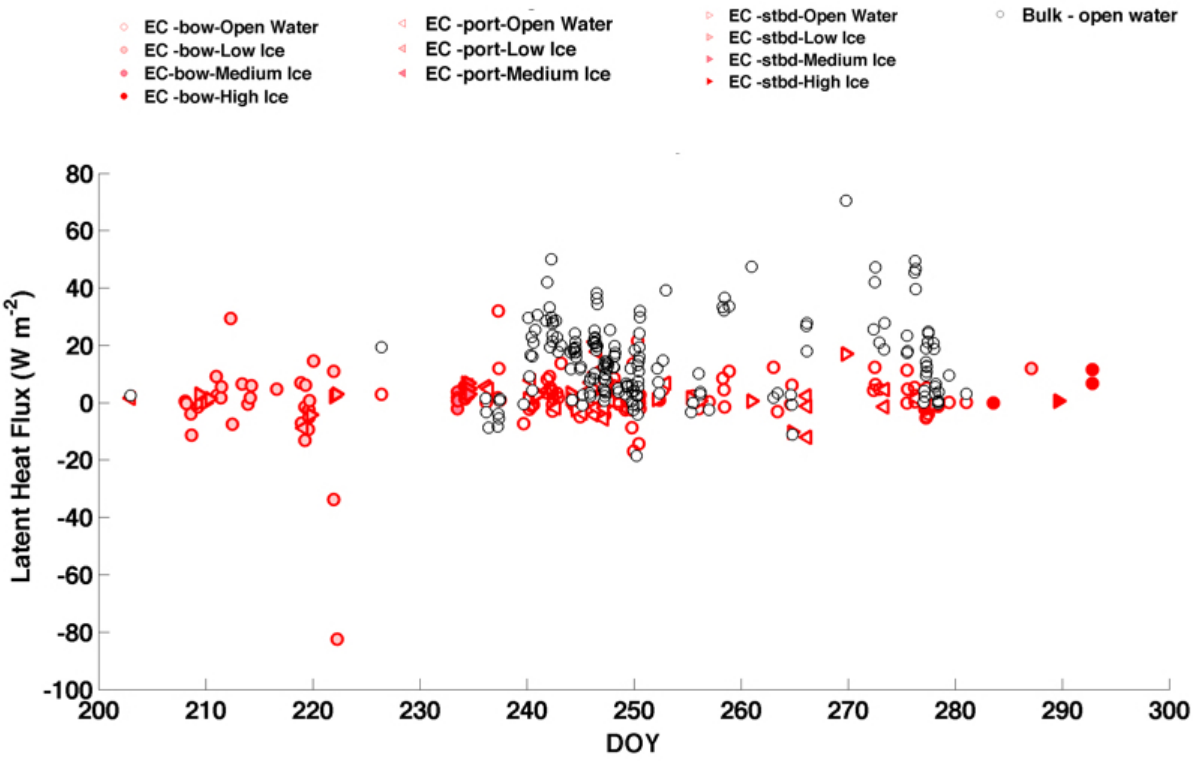

Figure 25. Scatter plots of each screened 20-minute period for EC (black) and bulk (red) latent heat flux over the duration of the cruise. Circles denote wind coming off the bow, left triangles represent wind come from the portside and right triangles represent wind coming from the starboard side. Sea ice concentration is indicated by the color. The darker, the higher ice concentration.

momentum fluxes were well correlated (r=0.72), however the EC approach tended to overestimate the flux relative to the bulk formulation (MAE of 0.04 Pa), and showed wider scatter (standard deviation of 0.08 vs. 0.06 for the bulk approach). The approaches tended to diverge for periods of higher shear (**Figure 26**).

Using the bulk approach, massive momentum flux arose in the north of Baffin Island, in the strait between Stefansson Island and Prince of Wales Island, and in Amundsen Gulf (**Figure 19**(a)). The EC-induced momentum flux reveals same trend but is less

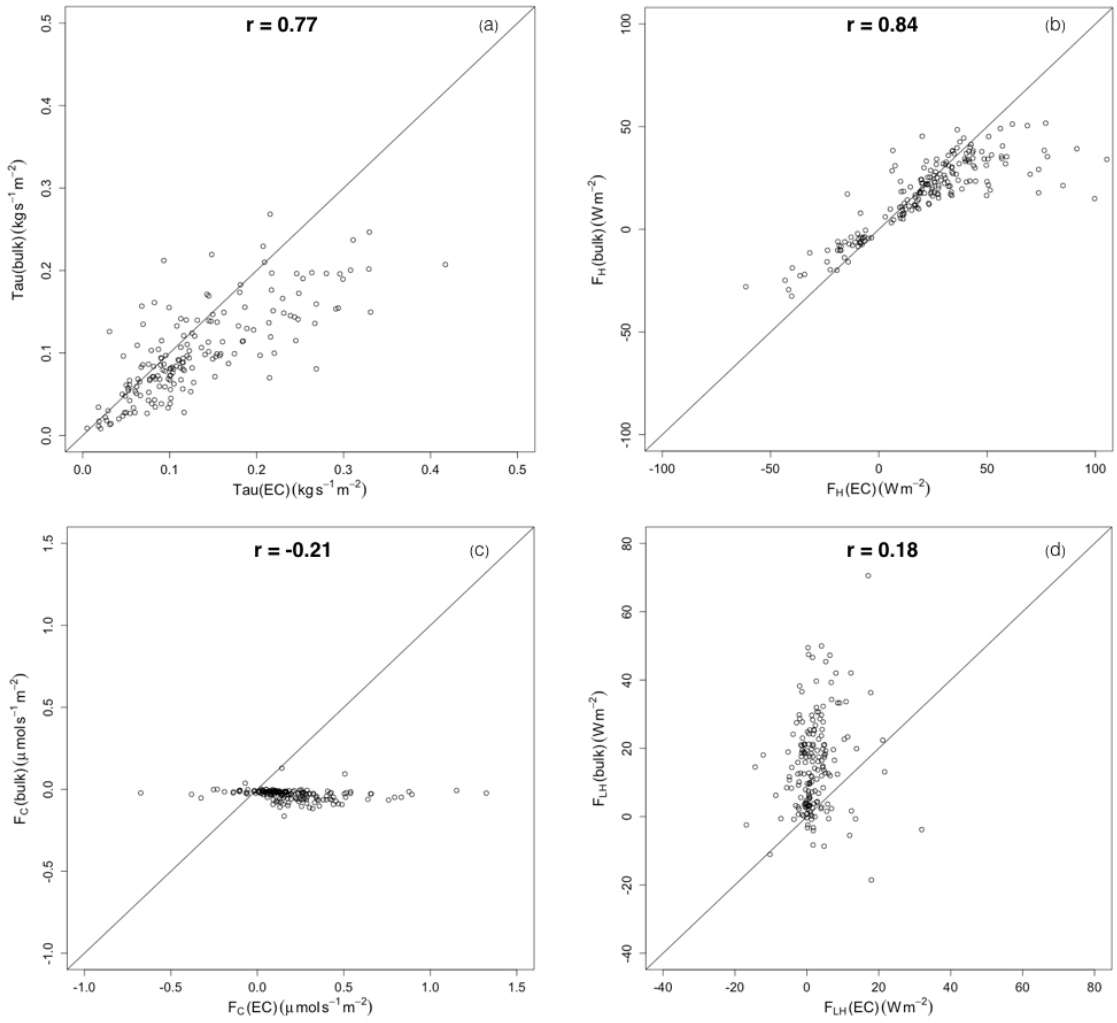

Figure 26. Fluxes of momentum (a), sensible heat (b) and CO_2 (c) estimated using the EC method plotted against fluxes derived from the bulk method for open water condition.

pronounced in Amundsen Gulf (**Figure 19**(b)). Data collected near Baffin Island was rejected during pre-processing for the EC method and are not available to be compared with the bulk approach. In the southwest of Beaufort Sea and the northwestern Banks

Table 8. Mean and standard deviation of momentum, sensible heat, latent heat and CO_2 fluxes using EC and bulk methods and the comparison of the two methods for open water

	EC		**Bulk**		**r**	**MAE**
	mean	std	mean	std		
Tau (kg s^{-1} m^{-2})	0.13	0.08	0.08	0.06	0.73	0.04
H (W m^{-2})	7.68	33.59	7.73	22.78	0.84	10.99
LH (W m^{-2})	1.93	6.72	12.31	16.03	0.11	14.55
CO_2 (μ mol s^{-1} m^{-2})	0.20	0.30	-0.02	0.15	0.08	0.26

Island, momentum flux using the EC method is shown to be greater than using the bulk method.

The resulting sensible heat flux using both the EC and bulk approaches over the cruise is shown in **Figure 20**. In the southern Baffin Bay, stronger absorption by the sea is indicated using the bulk approach. In the middle of Beaufort Sea and in Amundsen Gulf, the EC approach reflects more significant upward heat exchanges.

Figure 23 (b) shows the sensible heat flux time series using the two approaches and exhibits close agreement with the correlation coefficient of 0.84 (**Table 8**). However, EC heat flux is distributed over a greater range with standard deviation of 33.59 relative to that of 22.78 for H_{bulk}(**Table 5**) and gives more positive flux than H_{bulk}. The time series also reflects pronounced heat loss by the atmosphere on Day 243 and Day 259 and is shown to be associated with large air-sea temperature gradient (**Figure 18**). Overestimated EC sensible heat flux is encountered on Day 242, Day 243, Day 259-261 and Day 276 when apparent wind speed reaches 12 m/s, 15 m/s, 17 m/s and 19 m/s (**Figure 17**).

Shown on maps in **Figure 21**, the CO_2 flux using the EC method demonstrates much greater CO_2 emission to the atmosphere in Amundsen Gulf. The greatest disparate was found in CO_2 (**Figure 24**) and latent heat (**Figure 25**) fluxes. As shown in **Figure 24**, throughout the first 60 days over the cruise, CO_2 flux estimated using bulk method appears to be slightly under-saturated however the EC CO_2 flux is scattered and more of an oversaturation. Only from Day 274 to Day 280, the bulk derived CO_2 flux is found to be a strong oversaturation and agrees relatively well with EC CO_2 flux. Worth noticing is that the EC latent heat flux and the bulk latent heat flux seem to be complementary to its CO_2 counterpart.

4. DISCUSSION

4.1. UNCERTAINTIES IN EC METHOD

Since the EC approach is very sensitive to errors from different sources, the EC fluxes need to be resolved with great care. Platform motion and flow distortion are considered to have a greater impact on momentum flux than on scalar fluxes (Miller et al. 2010). Days with excessive momentum flux seem to be associated with high apparent wind speed indicating the chance of immense flow distortion. Sensible heat flux also suffers from flow distortion. Greater overestimation is also found in sensible heat flux when apparent wind speed is large. Although efforts were made to correct for the overestimation, the bias was not entirely eliminated.

A few studies have showed excessive wind flux over research vessels (Edson et al. 1998; Pedreros 2003; Edson et al. 2013; Landwehr et al. 2015; Prytherch et al. 2015), in general consensus with our results. To elaborate, Landwehr et al. (2015) reported errors in the estimation of tilt angles using the conventional motion correction routine because the vertical wind speed should be a function of relative wind speed not the true wind speed and the role of the wind is not accounted for in the equation. In addition, errors are found in measured relative wind direction. It was shown that for a relative wind direction range of ± 90°, the commonly accepted motion and tilt correction routine introduced an overestimation of up to 50% for friction velocity and up to 25% for heat flux (Landwehr et al. 2015). Prytherch et al. (2015) reported worse distortion of measurement taken from *RRS James Clark Ross* and pointed out that the magnitude of overestimation has a strong relevance to the specific platforms and installations, thus making it difficult to predict. Our tilt correction results also revealed that the tilt correction on EC data for portside winds seems to be the most effective however for bow-on wind the tilt was not successfully corrected. This is possibly due to the resolved tilt angles were biased caused by the very distorted flow over the bow.

The covariance of CO_2 concentration and the vertical wind component can serve as a noise filter when the CO_2 sensor is not motion sensitive (Miller et al. 2010). However, we did see residual of motion contamination in both vertical wind and CO_2 spectra respectively and this may lead to overestimated flux.

It appears that our EC system did not satisfactorily resolve the CO_2 and latent heat flux compared against the bulk derived results. It is possible that the humidity crosstalk largely contaminates the CO_2 flux measurement. Miller et al., (2010) suggest that the

resulting error in the CO_2 flux resulting from the errors in the latent heat flux needed for the density correction to CO_2 flux for un-dried air approach the magnitude of the CO_2 flux. Additionally, ΔpCO_2 typically was within ±40 μatm resulting from small air-sea CO_2 gradients, and therefore small potential for appreciable CO_2 exchange. The average ΔpCO_2 is -47.12 μatm over our entire cruise.

4.2. UNCERTAINTIES IN BULK METHOD

At extremely low wind conditions, fluxes may arise from large convective eddies that cannot be satisfactorily parameterized and it is more likely to get reliable CO_2 flux under large ΔpCO_2 and high wind speed conditions (McGillis et al. 2001). However, at high wind speed, there are other controlling parameters associated with sea state for transfer velocity other than wind speed (McGillis et al. 2001).

For CO_2 bulk estimation, an important term in the bulk equation is k_{CO_2}, which varies greatly using different parameterizations (Rutgersson et al. 2008; Mørk et al. 2014). It also remains controversy that transfer velocity is wind speed dependent (Liss and Merlivat 1986; Jacobs et al. 1999; Nightingale et al. 2000; Wanninkhof and McGillis 1999; Woolf 2005; Weiss et al. 2007). Notably, at mid to high wind speed, the gas transfer exhibits a nonlinear relationship to wind speed (Wanninkhof 1992; Wanninkhof and McGillis 1999; McGillis et al. 2001). In addition, as the transfer velocity is sensitive to seawater temperature and the skin temperatures were cooler than the bulk seawater temperature measured at 5 meters under water, the resulting bulk CO_2 flux is likely to be overestimated (McGillis and Wanninkhof 2006).

4.3. SEA ICE IMPACT

Another factor in air-sea fluxes is the sea ice. Compared to open water, the sea ice cover could add roughness to the surface. On Day 282 and Day 290 when ice concentration was extremely high and the wind was from port and starboard side, the EC momentum flux was found to be greater than the bulk momentum flux. This may be attributed to the increased surface roughness. Heat flux seems to scatter when there was bergy-ice dominated water during the ice-melting period from Day 210 to Day 222. The scatter may be associated with the complicated mechanism happening during melt pond formation (Parmentier et al. 2013). However, due to the very limited periods available with present sea ice, it is difficult to make a solid sea ice analysis for momentum and sensible heat flux.

Some researchers have argued that sea ice prevents the air-sea exchange of CO_2 and reduce the magnitude of CO_2 fluxes (Bates and Mathis 2009; Takahashi et al. 2009). However, the CO_2 dynamics is complex and the role sea ice act on air-sea CO_2 exchange remains largely unclear (Parmentier et al. 2013). For Day 216, Day 220-211, Day 235-237, Day 251 and Day 260, sea ice was present and the EC CO_2 fluxes scatter mostly above zero whereas CO_2 fluxes using the bulk approach appear to be all negative and relatively high in magnitude. Due to the interference of water vapour, it is difficult to find the influence of sea ice on CO_2 flux.

5. CONCLUSIONS

It is reflected in the co-spectra and when compared against the bulk fluxes that flow distortion was an issue for momentum flux, especially. The magnitude of flow distortion was shown to be very sensitive to relative wind direction. It appeared that the commonly accepted screening for relative wind direction is not applicable for our specific vessel and installation. The estimated EC momentum and sensible heat flux are overall greater than bulk-derived flux. There is more noticeable disparity using the two approaches for CO_2 and latent heat flux. This is not unexpected as data from different systems adds to the uncertainties and the crosstalk effect was strong. The analysis of sea ice impact on turbulent flux is hampered due to deficiency of in screened data set.

Conclusions can be drawn from our results that the EC application onboard Amundsen is feasible but improvements could be made to the setup as well as data post-processing.

6. FUTURE CONSIDERATIONS

For the EC application on Amundsen, we suggest to extend the mast vertically and reach further out. In cases when flow distortion is unavoidable, remedy could be made in data-post processing. Landwehr et al. (2015) proposed an alternative approach for motion correction and tilt angles estimation that carefully accounted for errors in classical motion correction attributed to flow distortion. Prytherch et al. (2015) pointed out that the observed mean wind may be biased because of acceleration and deceleration of flow and the measurement height would be lower than the instrument height due to upstream flow.

A motion-scale correction (MSC) algorithm was then introduced and applied. Results showed a significant decrease (up to 30%) in the drag coefficient for wind speeds greater than 7 m/s. As we are in a similar situation as Landwehr et al. (2015) and Prytherch et al. (2015), to bring our processing to higher quality, it would be worthwhile adopting their techniques.

As flow distortion related bias was found in both the EC and the bulk methods, it is desirable to bring the well-established ID approach into future research. Filter design, for example, band-pass filter that can model at both low and high frequencies, may assist to build better-shaped co-spectra that are more comparable to the theoretical ones. Alternatively, calculating the flux discrepancy between the EC measured individual 20-min period and that predicted by theory and set an appropriate threshold for co-spectra screening could be hassle-free and more objective. Variation in stability was ignored in this analysis and may be add to categorize data. As little is know about the impact of sea ice on CO_2 flux, experiments under extreme conditions should be carry out to make more data available for research.

To reduce the humidity crosstalk on CO_2, Butterworth and Miller (2015) has used a moisture exchanger to dry the sample air. Reasonable agreement was reached in CO_2 flux between their augmented EC system and flux parameterizations. This may be worth trying in our future cruises.

From the signal processing point of view, noise may be eliminated in data post processing. The adaptive filter that is capable of correcting the fluxes according to an optimization algorithm by modeling the theoretical co-spectra curves may be worth bringing into future research.

Reference:

Anderson, R.J. 1993. “A Study of Wind Stress and Heat Flux over the Open Ocean by the Inertial-Dissipation Method.” *Journal of Physical Oceanography* 23: 2153–61.

Andreas, E. L., and B. Murphy. 1986. “Bulk Transfer Coefficients for Heat and Momentum over Leads and Polynyas.” *Journal of Physical Oceanography*. doi:10.1175/1520-0485(1986)016<1875:BTCFHA>2.0.CO;2.

Andreas, E. L., C. A. Paulson, R. M. William, R. W. Lindsay, and J. A. Businger. 1979. “The Turbulent Heat Flux from Arctic Leads.” *Boundary-Layer Meteorology* 17 (1): 57–91. doi:10.1007/BF00121937.

Andreas, Edgar L, and Benjamin A Cash. 1999. “Convective Heat Transfer over Wintertime Leads and Polynyas the Value Typically Reported over the Open Ocean at Lower Latitudes , Fetches Much” 104 (Cll): 721–34.

Andreas, Edgar L., P. Ola G. Persson, and Jeffrey E. Hare. 2008. “A Bulk Turbulent Air-Sea Flux Algorithm for High-Wind, Spray Conditions.” *Journal of Physical Oceanography* 38: 1581–96. doi:10.1175/2007JPO3813.1.

Aubinet, Marc, Timo Vesala, and Dario Papale. 2012. *Eddy Covariance*. *A Practical Guide to Measurement and Data Analysis*. doi:10.1007/978-94-007-2351-1.

Barlow, Janet F., James Harrison, Alan G. Robins, and Curtis R. Wood. 2011. “A Wind-Tunnel Study of Flow Distortion at a Meteorological Sensor on Top of the BT Tower, London, UK.” *Journal of Wind Engineering and Industrial Aerodynamics* 99 (9). Elsevier: 899–907. doi:10.1016/j.jweia.2011.05.001.

Bates, N. R., and J. T. Mathis. 2009. “The Arctic Ocean Marine Carbon Cycle:

Evaluation of Air-Sea CO_2 Exchanges, Ocean Acidification Impacts and Potential Feedbacks." *Biogeosciences Discussions* 6 (4): 6695–6747. doi:10.5194/bgd-6-6695-2009.

Bates, Nicholas R., S. Bradley Moran, Dennis A. Hansell, and Jeremy T. Mathis. 2006. "An Increasing CO_2 Sink in the Arctic Ocean due to Sea-Ice Loss." *Geophysical Research Letters* 33 (23): 1–7. doi:10.1029/2006GL027028.

Blanc, Theodore V. 1985. "Variation of Bulk-Derived Surface Flux, Stability, and Roughness Results Due to the Use of Different Transfer Coefficient Schemes." *Journal of Physical Oceanography* 15 (6): 650–69. doi:10.1175/1520-0485(1985)015<0650:VOBDSF>2.0.CO;2.

Blomquist, Byron W., Barry J. Huebert, Christopher W. Fairall, Ludovic Bariteau, James B. Edson, Jeffrey E. Hare, and Wade R. McGillis. 2014. "Advances in Air-Sea CO_2 Flux Measurement by Eddy Correlation." *Boundary-Layer Meteorology* 152 (3): 245–76. doi:10.1007/s10546-014-9926-2.

Bourassa, Mark A., Sarah T. Gille, Cecilia Bitz, David Carlson, Ivana Cerovecki, Carol Anne Clayson, Meghan F. Cronin, et al. 2013. "High-Latitude Ocean and Sea Ice Surface Fluxes: Challenges for Climate Research." *Bulletin of the American Meteorological Society* 94 (3): 403–23. doi:10.1175/BAMS-D-11-00244.1.

Bourassa, Mark, Sarah Gille, Bitz Cecilia, David Carlson, Ivana Cerovecki, Meghan Cronin, Will Drennan, et al. 2011. "Outline: High Latitude Surface Fluxes: Requirements and Challenges for Climate Research," 1–25. http://www-pord.ucsd.edu/~sgille/highlat/hilatr_manuscript_v29s.pdf\npapers2://publication/uuid/C1385DE3-4053-427D-9519-6B7BD04DA296.

Bradley, F, and C Fairall. 2006. *A Guide to Making Climate Quality Meteorological and Flux Measurements at Sea*. *NOAA Technical Memorandum*. E:\Downloads\NOAA\fluxhandbook_NOAA-TECH PSD-311v3.pdf.

Brunke, Michael A., Mingyu Zhou, Xubin Zeng, and Edgar L. Andreas. 2006. "An Intercomparison of Bulk Aerodynamic Algorithms Used over Sea Ice with Data from the Surface Heat Budget for the Arctic Ocean (SHEBA) Experiment." *Journal of Geophysical Research: Oceans* 111 (9). doi:10.1029/2005JC002907.

Burba, G, and D Anderson. 2010. "Eddy Covariance Flux Measurements." *Ecological Applications* 18 (6): 211. http://www.ncbi.nlm.nih.gov/pubmed/18767616.

Burba, George, Andres Schmidt, Russell L. Scott, Taro Nakai, James Kathilankal, Gerardo Fratini, Chad Hanson, et al. 2012. "Calculating CO2 and H2O Eddy Covariance Fluxes from an Enclosed Gas Analyzer Using an Instantaneous Mixing Ratio." *Global Change Biology* 18 (1): 385–99. doi:10.1111/j.1365-2486.2011.02536.x.

Butterworth, Brian J., and Scott D. Miller. 2015. "Automated Underway Eddy Covariance System for Air-Sea Momentum, Heat, and CO2 Fluxes in the Southern Ocean." *Journal of Atmospheric and Oceanic Technology*, in review. https://www.dropbox.com/s/9p9y7nzcz90ees5/JTECH-S-15-00202.pdf?dl=0.

Cava, D., D. Contini, a. Donateo, and P. Martano. 2008. "Analysis of Short-Term Closure of the Surface Energy Balance above Short Vegetation." *Agricultural and Forest Meteorology* 148 (1): 82–93. doi:10.1016/j.agrformet.2007.09.003.

Comiso, Josefino C., Claire L. Parkinson, Robert Gersten, and Larry Stock. 2008. "Accelerated Decline in the Arctic Sea Ice Cover." *Geophysical Research Letters* 35

(1): 1–6. doi:10.1029/2007GL031972.

Coppin, P.A., and K.J. Taylor. 1983. “A Three-Component Anemometer/thermometer Micrometeorological.” *Boundary-Layer Meteorology* 27: 27–42.

Deyer, A J. 1981. “Flow Distorsion by Supporting Structures.” *CSIRO Division of Atmospheric Physics, Australia*. CSIRO Division of Atmospheric Physics.

Dupuis, H., C. Guerin, D. Hauser, A. Weill, P. Nacass, W. M. Drennan, S. Cloché, and H. C. Graber. 2003. “Impact of Flow Distortion Corrections on Turbulent Fluxes Estimated by the Inertial Dissipation Method during the FETCH Experiment on R/V L’Atalante.” *Journal of Geophysical Research C: Oceans* 108 (3): 12–1 . doi:10.1029/2001JC001075.

Edson, J. B., C. W. Fairall, L. Bariteau, C. J. Zappa, A. Cifuentes-Lorenzen, W. R. McGillis, S. Pezoa, J. E. Hare, and D. Helmig. 2011. “Direct Covariance Measurement of CO_2 Gas Transfer Velocity during the 2008 Southern Ocean Gas Exchange Experiment: Wind Speed Dependency.” *Journal of Geophysical Research* 116: C00F10. doi:10.1029/2011JC007022.

Edson, J. B., C. W. Fairall, P. G. Mestayer, and S. E. Larsen. 1991. “A Study of the Inertial-Dissipation Method for Computing Air-Sea Fluxes.” *Journal of Geophysical Research* 96 (C6): 10689. doi:10.1029/91JC00886.

Edson, J. B., a. a. Hinton, K. E. Prada, J. E. Hare, and C. W. Fairall. 1998. “Direct Covariance Flux Estimates from Mobile Platforms at Sea*.” *Journal of Atmospheric and Oceanic Technology* 15 (2): 547–62.

Edson, James B., Venkata Jampana, Robert a. Weller, Sebastien P. Bigorre, Albert J. Plueddemann, Christopher W. Fairall, Scott D. Miller, Larry Mahrt, Dean Vickers,

and Hans Hersbach. 2013. “On the Exchange of Momentum over the Open Ocean.” *Journal of Physical Oceanography* 43 (8): 1589–1610. doi:10.1175/JPO-D-12-0173.1.

Else, B. G. T., T. N. Papakyriakou, R. J. Galley, W. M. Drennan, L. A. Miller, and H. Thomas. 2011. “Wintertime CO_2 Fluxes in an Arctic Polynya Using Eddy Covariance: Evidence for Enhanced Air-Sea Gas Transfer during Ice Formation.” *Journal of Geophysical Research* 116: C00G03. doi:10.1029/2010JC006760.

Eric W. Schulz, B. G. Sanderson, E. F. Bradley. 2005. “Motion Correction for Shipborne Turbulence Sensors.” *Journal of Atmospheric and Oceanic Technology* 22 (1): 55–69.

Fairall, C. W., E. F. Bradley, J. E. Hare, A. A. Grachev, and J. B. Edson. 2003. “Bulk Parameterization of Air-Sea Fluxes: Updates and Verification for the COARE Algorithm.” *Journal of Climate* 16 (4): 571–91. doi:10.1175/1520-0442(2003)016<0571:BPOASF>2.0.CO;2.

Fairall, C. W., J. E. Hare, J. B. Edson, and W. McGillis. 2000. “Parameterization and Micrometeorological Measurement of Air–Sea Gas Transfer.” *Boundary-Layer Meteorology* 96 (1): 63–106. doi:10.1023/A:1002662826020.

Fairall, C. W., and S. E. Larsen. 1986. “Inertial-Dissipation Methods and Turbulent Fluxes at the Air-Ocean Interface.” *Boundary-Layer Meteorology* 34 (3): 287–301. doi:10.1007/BF00122383.

Fan, Song-miao, S C Wofsy, Peter S Bakwin, Daniel J Jacob, and D R Fitzjarrald. 1990. “Atmosphere-Biosphere Exchange of CO2 and 03 in the Central Amazon Forest.” *Journal of Geophysical Research* 95: 851–64.

Foken, Thomas. 2008. *Micrometeorology*. *English*.

Fujitani, Tokunosuke. 1981. “Direct Measurement of Turbulent Fluxes over the Sea During AMTEX.” *Meteorology and Geophysics* 32 (3): 119–34.

Gash, J.H.C., and A.J. Dolman. 2003. “Sonic Anemometer (Co)sine Response and Flux Measurement.” *Agricultural and Forest Meteorology* 119 (3-4): 195–207. doi:10.1016/S0168-1923(03)00137-0.

Geilfus, N. X., R. J. Galley, O. Crabeck, T. Papakyriakou, J. Landy, J. L. Tison, and S. Rysgaard. 2015. “Inorganic Carbon Dynamics of Melt-Pond-Covered First-Year Sea Ice in the Canadian Arctic.” *Biogeosciences* 12 (6): 2047–61. doi:10.5194/bg-12-2047-2015.

Geilfus, N. X., J. L. Tison, S. F. Ackley, R. J. Galley, S. Rysgaard, L. A. Miller, and B. Delille. 2014. “Sea Ice pCO2 Dynamics and Air-Ice CO2 Fluxes during the Sea Ice Mass Balance in the Antarctic (SIMBA) Experiment – Bellingshausen Sea, Antarctica.” *Cryosphere* 8 (6): 2395–2407. doi:10.5194/tc-8-2395-2014.

Ibrom, Andreas, Ebba Dellwik, Henrik Flyvbjerg, Niels Otto Jensen, and Kim Pilegaard. 2007. “Strong Low-Pass Filtering Effects on Water Vapour Flux Measurements with Closed-Path Eddy Correlation Systems.” *Agricultural and Forest Meteorology* 147 (3-4): 140–56. doi:10.1016/j.agrformet.2007.07.007.

Ibrom, Andreas, Ebba Dellwik, S??ren Ejling Larsen, and Kim Pilegaard. 2007. “On the Use of the Webb-Pearman-Leuning Theory for Closed-Path Eddy Correlation Measurements.” *Tellus, Series B: Chemical and Physical Meteorology* 59 (5): 937–46. doi:10.1111/j.1600-0889.2007.00311.x.

Iwata, T., K. Yoshikawa, Y. Higuchi, T. Yamashita, S. Kato, and E. Ohtaki. 2005. “The

Spectral Density Technique for the Determination of CO2 Flux Over the Ocean." *Boundary-Layer Meteorology* 117 (3): 511–23. doi:10.1007/s10546-005-2773-4.

Jacobs, Cor M J, W I M Kohsiek, and Wiebe A Oost. 1999. "Air-Sea Fluxes and Transfer Velocity of CO_2 over the North Sea: Results from ASGAMAGE." *Tellus B* 51 (3): 629–41.

Kaimal, J C, and J J Finnigan. 1994. *Atmospheric Boundary Layer Flows: Their Structure and Measurement*. *Book*. Vol. 72. doi:10.1016/0021-9169(95)90002-0.

Kaimal, J. C., and D. A. Haugen. 1969. "Kaimal Haugen 1969.pdf." *Journal of Applied Meteorology* 8: 460–62.

Kaimal, J. C., J. C. Wyngaard, Y. Izumi, and O. R. Coté. 1972. "Spectral Characteristics of Surface-Layer Turbulence." *Quarterly Journal of the Royal Meteorological Society* 98: 563–89. doi:10.1002/qj.49709841707.

Kohsiek, W. 2000. "Water Vapor Cross-Sensitivity of Open Path H2O/CO2 Sensors." *Journal of Atmospheric and Oceanic Technology* 17 (3): 299–311. doi:doi:10.1175/1520- 0426(2000)017<0299:WVCSOO>2.0.CO;2.

Kolmogorov, A N. 1941. "The Local Structure of Turbulance in Incompressible Viscous Fluid for Very Large Reynolds Numbers." *Doklady ANSSSR* 30 (1890): 301–4. doi:10.1098/rspa.1991.0075.

Kondo, Fumiyoshi, and Osamu Tsukamoto. 2007. "Air-Sea CO2 Flux by Eddy Covariance Technique in the Equatorial Indian Ocean." *Journal of Oceanography* 63 (1999): 449–56. doi:10.1007/s10872-007-0040-7.

Kurtz, N T, T Markus, S L Farrell, D L Worthen, and L N Boisvert. 2011. "Observations of Recent Arctic Sea Ice Volume Loss and Its Impact on Ocean - Atmosphere

Energy Exchange and Ice Production" 116 (January): 1–19. doi:10.1029/2010JC006235.

Landwehr, Sebastian, Niall O'Sullivan, and Brian Ward. 2015. "Direct Flux Measurements from Mobile Platforms at Sea: Motion and Airflow Distortion Corrections Revisited." *Journal of Atmospheric and Oceanic Technology* 32 (6): 1163–78. doi:10.1175/JTECH-D-14-00137.1.

Lee, Xuhui, William J. Massman, and Beverly Law. 2005. *Handbook of Micrometeorology*. doi:10.1007/1-4020-2265-4.

Leuning, Ray. 2004. "Chapter 6 MEASUREMENTS OF TRACE GAS FLUXES IN THE ATMOSPHERE USING EDDY COVARIANCE : WPL CORRECTIONS REVISITED." In *Handbook of Micrometeorology*, 250.

Leuning, Ray, and Murray J. Judd. 1996. "The Relative Merits of Open- and Closed-Path Analysers for Measurement of Eddy Fluxes." *Global Change Biology* 2: 241–53. doi:10.1111/j.1365-2486.1996.tb00076.x.

Leuning, Ray, and John Moncrieff. 1990a. "Eddy-Covariance CO2 Flux Measurements Using Open-and Closed-Path CO2 Analysers: Corrections for Analyser Water Vapour Sensitivity and Damping of Fluctuations in Air Sampling Tubes." *Boundary-Layer Meteorology* 53 (1): 63–76. doi:10.1007/BF00122463.

———. 1990b. "Eddy-Covariance CO2 Flux Measurements Using Open- and Closed-Path CO2 Analysers: Corrections for Analyser Water Vapour Sensitivity and Damping of Fluctuations in Air Sampling Tubes." *Boundary-Layer Meteorology* 53 (1-2): 63–76. doi:10.1007/BF00122463.

Liss, P. S., and P. G. Slater. 1974. "Flux of Gases across the Air-Sea Interface." *Nature*

247: 181–84. doi:10.1038/247181a0.

Liu, L, T J Wang, Z H Sun, Q G Wang, B L Zhuang, Y Han, and S Li. 2012. "Eddy Covariance Tilt Corrections over a Coastal Mountain Area in South-East China: Significance for near-Surface Turbulence Characteristics." *Advances in Atmospheric Sciences* 29 (6): 1264–78. doi:DOI 10.1007/s00376-012-1052-9.

Loose, B., W. R. McGillis, D. Perovich, C. J. Zappa, and P. Schlosser. 2014. "A Parameter Model of Gas Exchange for the Seasonal Sea Ice Zone." *Ocean Science* 10 (1): 17–28. doi:10.5194/os-10-17-2014.

Manabe, Syukuro, and Ronald J. Stouffer. 1980. "Sensitivity of a Global Climate Model to an Increase of CO2 Concentration in the Atmosphere." *Journal of Geophysical Research* 85 (C10): 5529–54. doi:10.1029/JC085iC10p05529.

Marcq, S, and J Weiss. 2012. "The Cryosphere Influence of Sea Ice Lead-Width Distribution on Turbulent Heat Transfer between the Ocean and the Atmosphere," 143–56. doi:10.5194/tc-6-143-2012.

Massman, William. 2004. "Chapter 7 CONCERNING THE MEASUREMENT OF ATMOSPHERIC TRACE GAS FLUXES WITH OPEN- AND CLOSED-PATH EDDY COVARIANCE SYSTEM : THE WPL TERMS AND SPECTRAL ATTENUATION." *Handbook of Micrometeorology* 29: 133–60. doi:10.1007/1-4020-2265-4_7.

McGillis, W R, J B Edson, J E Hare, and C W Fairall. 2001. "Direct Covariance Air-Sea CO2 Fluxes." *Journal of Geophysical Research* 106 (C8). AGU: 16729–45. http://dx.doi.org/10.1029/2000JC000506.

McGillis, Wade R., and J. B. Edson. 2001. "Direct Covairance Air-Sea CO2 Fluxes."

Journal of Geophysical Research 106.

McGillis, Wade R., and Rik Wanninkhof. 2006. “Aqueous CO2 Gradients for Air-Sea Flux Estimates.” *Marine Chemistry* 98 (1): 100–108. doi:10.1016/j.marchem.2005.09.003.

Miller, S D, C Marandino, and E S Saltzman. 2010. “Ship-Based Measurement of Air-Sea CO2 Exchange by Eddy Covariance.” *Journal of Geophysical Research-Atmospheres* 115 (D2): - ST – Ship – based measurement of air – sea CO2 exch. doi:10.1029/2009JD012193.

Miller, Scott D., Tihomir S. Hristov, James B. Edson, and Carl a. Friehe. 2008. “Platform Motion Effects on Measurements of Turbulence and Air–Sea Exchange over the Open Ocean.” *Journal of Atmospheric and Oceanic Technology* 25 (9): 1683–94. doi:10.1175/2008JTECHO547.1.

Mitsuta, Y, and T Fujitani. 1974. “DIRECT MEASUREMENT OF TURBULENT SHIP FLUXES This Paper Describes a Method for the Direct Measurement of Turbulent Fluxes of Heat and Water Vapor from a Cruising Ship over the Open Ocean . A Ship Is the Only Feasible Platform for Open-Ocean Surface Flux Me” 6: 203–17.

Moat, Bengamin I., Margaret J. Yelland, Robin W. Pascal, and Anthony F. Molland. 2005. “An Overview of the Airflow Distortion at Anemometer Sites on Ships.” *International Journal of Climatology* 25 (7): 997–1006. doi:10.1002/joc.1177.

———. 2006. “Quantifying the Airflow Distortion over Merchant Ships. Part I: Validation of a CFD Model.” *Journal of Atmospheric and Oceanic Technology* 23 (3): 341–50. doi:10.1175/JTECH1858.1.

Moncrieff, J.B., J.M. Massheder, H. de Bruin, J. Elbers, T. Friborg, B. Heusinkveld, P.

Kabat, S. Scott, H. Soegaard, and A. Verhoef. 1997. “A System to Measure Surface Fluxes of Momentum, Sensible Heat, Water Vapour and Carbon Dioxide.” *Journal of Hydrology* 188-189: 589–611. doi:10.1016/S0022-1694(96)03194-0.

Montgomery, R. B. 1948. “Vertical Eddy Flux of Heat in the Atmosphere.” *Journal of Meteorology* 5 (6): 265–74. doi:10.1175/1520-0469(1948)005<0265:VEFOHI>2.0.CO;2.

Mørk, Eva Thorborg, Lise Lotte Sørensen, Bjarne Jensen, and Mikael K. Sejr. 2014. “Air-Sea CO2 Gas Transfer Velocity in a Shallow Estuary.” *Boundary-Layer Meteorology* 151 (1): 119–38. doi:10.1007/s10546-013-9869-z.

Nakai, Taro, and Kou Shimoyama. 2012. “Ultrasonic Anemometer Angle of Attack Errors under Turbulent Conditions.” *Agricultural and Forest Meteorology* 162-163. Elsevier B.V.: 14–26. doi:10.1016/j.agrformet.2012.04.004.

Nakai, Taro, M. K. Van Der Molen, J. H C Gash, and Yuji Kodama. 2006. “Correction of Sonic Anemometer Angle of Attack Errors.” *Agricultural and Forest Meteorology* 136: 19–30. doi:10.1016/j.agrformet.2006.01.006.

Nightingale, Philip D., Gill Malin, Cliff S. Law, Andrew J. Watson, Peter S. Liss, Malcolm I. Liddicoat, Jacqueline Boutin, and Robert C. Upstill-Goddard. 2000. “In Situ Evaluation of Air-Sea Gas Exchange Parameterizations Using Novel Conservative and Volatile Tracers.” *Global Biogeochemical Cycles* 14 (1): 373. doi:10.1029/1999GB900091.

Norman, Maria, Anna Rutgersson, Lise Lotte Sørensen, and Erik Sahlée. 2012. “Methods for Estimating Air–Sea Fluxes of CO2 Using High-Frequency Measurements.” *Boundary-Layer Meteorology* 144 (3): 379–400. doi:10.1007/s10546-012-9730-9.

O'Sullivan, N., S. Landwehr, and B. Ward. 2013. "Mapping Flow Distortion on Oceanographic Platforms Using Computational Fluid Dynamics." *Ocean Science* 9 (5): 855–66. doi:10.5194/os-9-855-2013.

Obukhov, A. M. 1951. "Characteristics of the Micro-Structure of the Wind in the Surface Layer of the Atmosphere." *Izv AN SSSR, Ser Geofiz* 3: 49–68.

Ocean, Southern. 2014. "Journal of Atmospheric and Oceanic Technology Automated Underway Eddy Covariance System for Air-Sea Momentum , Heat , and CO2 Fluxes in the Southern Ocean Corresponding Author Address : Scott D . Miller , Atmospheric Sciences Research Center ,."

Ohtaki, E., and T. Matsui. 1982. "Infrared Device for Simultaneous Measurement of Fluctuations of Atmospheric Carbon Dioxide and Water Vapor." *Boundary-Layer Meteorology* 24: 109–19. doi:10.1007/BF00121803.

Oost, W A, C Fairall, J Edson, S Smith, R Anderson, J Wills, K Katsaros, and J DeCosmo. 1994. "Flow Distortion Calculations and Their Application in HEXMAX." *J.\ Atmospheric and Oceanic Technology*. 11: 366–86.

OWER, E., and R.C. PANKHURST. 1977. *The Measurement of Air Flow*. *The Measurement of Air Flow*. doi:10.1016/B978-0-08-021281-4.50011-7.

P.S.Liss, and L.Merlivat. 1986. "Air-Sea Gas Exchange Rates Introduction and Synthesis." *Role of Air-Sea Exchange in Geochemical Cycling*, 113–27. doi:10.1007/978-94-009-4738-2_5.

Parmentier, Frans-Jan W., Torben R. Christensen, Lise Lotte Sørensen, Søren Rysgaard, a. David McGuire, Paul a. Miller, and Donald a. Walker. 2013. "The Impact of Lower Sea-Ice Extent on Arctic Greenhouse-Gas Exchange." *Nature Climate*

Change 3 (3). Nature Publishing Group: 195–202. doi:10.1038/nclimate1784.

Pedreros, R. 2003. "Momentum and Heat Fluxes via the Eddy Correlation Method on the R/V L'Atalante and an ASIS Buoy." *Journal of Geophysical Research* 108 (C11): 3339. http://doi.wiley.com/10.1029/2002JC001449.

Pierrot, Denis, Craig Neill, Kevin Sullivan, Robert Castle, Rik Wanninkhof, Heike Lüger, Truls Johannessen, Are Olsen, Richard a. Feely, and Catherine E. Cosca. 2009. "Recommendations for Autonomous Underway pCO2 Measuring Systems and Data-Reduction Routines." *Deep-Sea Research Part II: Topical Studies in Oceanography* 56 (8-10): 512–22. doi:10.1016/j.dsr2.2008.12.005.

Polyakov, Igor V. 2002. "Observationally Based Assessment of Polar Amplification of Global Warming." *Geophysical Research Letters* 29 (18): 3–6. doi:10.1029/2001GL011111.

Pond, S., G. T. Phelps, J. E. Paquin, G. McBean, and R. W. Stewart. 1971. "Measurements of the Turbulent Fluxes of Momentum, Moisture and Sensible Heat over the Ocean." *Journal of the Atmospheric Sciences*. doi:10.1175/1520-0469(1971)028<0901:MOTTFO>2.0.CO;2.

Popinet, Stéphane, Murray J. Smith, and C Stevens. 2004. "Experimental and Numerical Study of the Turbulence Characteristics of Airflow around a Research Vessel." *Journal of Atmospheric and Oceanic Technology*, no. 1981: 1575–89.

Proakis, John G., and Dimitri G. Monolakis. 1996. "Digital Signal Processing: Principles, Algorithms and Applications," 1–42.

Prytherch, J., M. J. Yelland, I. M. Brooks, D. J. Tupman, R. W. Pascal, B. I. Moat, and S. J. Norris. 2015. "Motion-Correlated Flow Distortion and Wave-Induced Biases in

Air–sea Flux Measurements from Ships." *Atmospheric Chemistry and Physics* 15 (18): 10619–29. doi:10.5194/acp-15-10619-2015.

Prytherch, John, Margaret J. Yelland, Robin W. Pascal, Bengamin I. Moat, Ingunn Skjelvan, and Craig C. Neill. 2010. "Direct Measurements of the CO2 Flux over the Ocean: Development of a Novel Method." *Geophysical Research Letters* 37 (3): 1–5. doi:10.1029/2009GL041482.

Rutgersson, Anna, Maria Norman, Bernd Schneider, Heidi Pettersson, and Erik Sahlée. 2008. "The Annual Cycle of Carbon Dioxide and Parameters Influencing the Air–sea Carbon Exchange in the Baltic Proper." *Journal of Marine Systems* 74 (1-2). Elsevier B.V.: 381–94. doi:10.1016/j.jmarsys.2008.02.005.

Rysgaard, S??ren, J??rgen Bendtsen, Bruno Delille, Gerhard S. Dieckmann, Ronnie N. Glud, Hilary Kennedy, John Mortensen, Stathys Papadimitriou, David N. Thomas, and Jean Louis Tison. 2011. "Sea Ice Contribution to the Air-Sea CO2 Exchange in the Arctic and Southern Oceans." *Tellus, Series B: Chemical and Physical Meteorology* 63 (5): 823–30. doi:10.1111/j.1600-0889.2011.00571.x.

Rysgaard, S., J. Mortensen, T. Juul-Pedersen, L. L. Sørensen, K. Lennert, D. H. Søgaard, K. E. Arendt, M. E. Blicher, M. K. Sejr, and J. Bendtsen. 2012. "High Air-Sea CO 2 Uptake Rates in Nearshore and Shelf Areas of Southern Greenland: Temporal and Spatial Variability." *Marine Chemistry* 128-129. Elsevier B.V.: 26–33. doi:10.1016/j.marchem.2011.11.002.

Schotanus, P., F. T M Nieuwstadt, and H. a R De Bruin. 1983. "Temperature Measurement with a Sonic Anemometer and Its Application to Heat and Moisture Fluxes." *Boundary-Layer Meteorology* 26 (1): 81–93. doi:10.1007/BF00164332.

Schulz, Eric W., B. G. Sanderson, and E. F. Bradley. 2005. “Motion Correction for Shipborne Turbulence Sensors.” *Journal of Atmospheric and Oceanic Technology* 22 (1): 55–69. doi:10.1175/JTECH-1685.1.

Schulz, EW. 2005. “Motion Correction for Shipborne Turbulence Sensors.” *Journal of Atmospheric …* 22 (1974): 55–69. http://journals.ametsoc.org/doi/abs/10.1175/JTECH-1685.1.

Screen, James a, and Ian Simmonds. 2010. “The Central Role of Diminishing Sea Ice in Recent Arctic Temperature Amplification.” *Nature* 464 (7293): 1334–37. doi:10.1038/nature09051.

Screen, James A., Ian Simmonds, Clara Deser, and Robert Tomas. 2013. “The Atmospheric Response to Three Decades of Observed Arctic Sea Ice Loss.” *Journal of Climate* 26 (4): 1230–48. doi:10.1175/JCLI-D-12-00063.1.

Serreze, M C, A P Barrett, J C Stroeve, D N Kindig, and M M Holland. 2009. “The Emergence of Surface-Based {Arctic} Amplification.” *The Cryosphere* 3 (1): 11–19. doi:10.5194/tc-3-11-2009.

Serreze, Mark C., and Roger G. Barry. 2011. “Processes and Impacts of Arctic Amplification: A Research Synthesis.” *Global and Planetary Change* 77 (1-2). Elsevier B.V.: 85–96. doi:10.1016/j.gloplacha.2011.03.004.

Serreze, Mark C., and Jennifer A. Francis. 2006. “The Arctic Amplification Debate.” *Climatic Change* 76 (3-4): 241–64. doi:10.1007/s10584-005-9017-y.

Smith, Shawn R., Mark A. Bourassa, and Ryan J. Sharp. 1999. “Establishing More Truth in True Winds.” *Journal of Atmospheric and Oceanic Technology* 16 (7): 939–52. doi:10.1175/1520-0426(1999)016<0939:EMTITW>2.0.CO;2.

Smith, Stuart D. 1988. “Coefficients for Sea Surface Wind Stress, Heat Flux, and Wind Profiles as a Function of Wind Speed and Temperature.” *Journal of Geophysical Research: Oceans* 93 (C12): 15467–72. doi:10.1029/JC093iC12p15467.

Sørensen, Lise Lotte, and Søren E Larsen. “Atmosphere-Surface Fluxes of CO 2 Using Spectral Techniques,” 0–30.

Stull, R B. 1988. “An Introduction to Boundary Layer Meteorology.” *Book* 13: 666. doi:10.1007/978-94-009-3027-8.

Swinbank, W. C. 1951. “The Measurement of Vertical Transfer of Heat and Water Vapor By Eddies in the Lower Atmosphere.” *Journal of Meteorology* 8 (3): 135–45. doi:10.1175/1520-0469(1951)008<0135:TMOVTO>2.0.CO;2.

Takahashi, Taro, Jon Olafsson, John G. Goddard, David W. Chipman, and S. C. Sutherland. 1993. “And Nutrients in the High-Latitude Surface Oceans: A Comparative Study.” *Global Biogeochemical Cycles* 7 (4): 843. doi:10.1029/93GB02263.

Takahashi, Taro, Stewart C. Sutherland, Colm Sweeney, Alain Poisson, Nicolas Metzl, Bronte Tilbrook, Nicolas Bates, et al. 2002. “Global Sea-Air CO2 Flux Based on Climatological Surface Ocean pCO2, and Seasonal Biological and Temperature Effects.” *Deep-Sea Research Part II: Topical Studies in Oceanography* 49 (9-10): 1601–22. doi:10.1016/S0967-0645(02)00003-6.

Takahashi, Taro, Stewart C. Sutherland, Rik Wanninkhof, Colm Sweeney, Richard A. Feely, David W. Chipman, Burke Hales, et al. 2009. “Climatological Mean and Decadal Change in Surface Ocean pCO2, and Net Sea-Air CO2 Flux over the Global Oceans.” *Deep-Sea Research Part II: Topical Studies in Oceanography* 56

(8-10): 554–77. doi:10.1016/j.dsr2.2008.12.009.

Tison, Jean-Louis, Christian Haas, Marcia M Gowing, Suzanne Sleewaegen, and Alain Bernard. 2002. “Tank Study of Physico-Chemical Controls on Gas Content and Composition during Growth of Young Sea Ice.” *Journal of Glaciology* 48 (161): 177–91. doi:10.3189/172756502781831377.

Van Der Molen, M. K., J. H C Gash, and J. a. Elbers. 2004. “Sonic Anemometer (Co)sine Response and Flux Measurement: II. The Effect of Introducing an Angle of Attack Dependent Calibration.” *Agricultural and Forest Meteorology* 122: 95–109. doi:10.1016/j.agrformet.2003.09.003.

W.F. Weeks. 2010. *On Sea Ice by W.F. Weeks. University of Alaska Press, Fairbanks, 2010. No of Pages: Xv + 664. ISBN 978-1-60223-079-8 (Hardback). University of Alaska Press*.

Wanninkhof, R, and W R McGillis. 1999. “A Cubic Relationship between Air-sea CO2 Exchange and Wind Speed.” *Geophysical Research Letters* 26 (13): 1889–92. doi:10.1029/1999GL900363.

Wanninkhof, Rik. 1992. “Relationship Between Wind Speed and Gas Exchange.” *Journal of Geophysical Research* 97 (92): 7373–82. doi:10.1029/92JC00188.

Wanninkhof, Rik, William E. Asher, David T. Ho, Colm Sweeney, and Wade R. McGillis. 2009. “Advances in Quantifying Air-Sea Gas Exchange and Environmental Forcing*.” *Annual Review of Marine Science* 1 (1): 213–44. doi:10.1146/annurev.marine.010908.163742.

Webb, Ek, G Pearman, and R Leuning. 1980. “Correction of Flux Measurements for Density Effects due to Heat and Water Vapour Transfer.” *Quarterly Journal of the*

Meteorologic Society. http://onlinelibrary.wiley.com/doi/10.1002/qj.49710644707/abstract.

Weiss, Alexandra, Joachim Kuss, Gerhard Peters, and Bernd Schneider. 2007. "Evaluating Transfer Velocity-Wind Speed Relationship Using a Long-Term Series of Direct Eddy Correlation CO2 Flux Measurements." *Journal of Marine Systems* 66 (1-4): 130–39. doi:10.1016/j.jmarsys.2006.04.011.

Weiss, R.F. 1974. "Carbon Dioxide in Water and Seawater: The Solubility of a Non-Ideal Gas." *Marine Chemistry* 2 (3): 203–15. doi:10.1016/0304-4203(74)90015-2.

Wilczak, J. M., S. P. Oncley, and S. a. Stage. 2001. "Sonic Anemometer Tilt Correction Algorithms." *Boundary-Layer Meteorology* 99 (1): 127–50. doi:10.1023/A:1018966204465.

Wilczak, James M., Steven P. Oncley, and Steven a. Stage. 2001. "Sonic Anemometer Tilt Correction Algorithms." *Boundary-Layer Meteorology* 99 (1): 127–50. doi:10.1023/A:1018966204465.

Woolf, David K. 2005. "Parametrization of Gas Transfer Velocities and Sea-State-Dependent Wave Breaking." *Tellus, Series B: Chemical and Physical Meteorology* 57 (2): 87–94. doi:10.1111/j.1600-0889.2005.00139.x.

Yelland, M. J., B. I. Moat, R. W. Pascal, and D. I. Berry. 2002. "CFD Model Estimates of the Airflow Distortion over Research Ships and the Impact on Momentum Flux Measurements." *Journal of Atmospheric and Oceanic Technology* 19 (10): 1477–99. doi:10.1175/1520-0426(2002)019<1477:CMEOTA>2.0.CO;2.

Yelland, M. J., B. I. Moat, P. K. Taylor, R. W. Pascal, J. Hutchings, and V. C. Cornell. 1998. "Wind Stress Measurements from the Open Ocean Corrected for Airflow

Distortion by the Ship." *Journal of Physical Oceanography* 28 (1980): 1511–26. doi:10.1175/1520-0485(1998)028<1511:WSMFTO>2.0.CO;2.

Yelland, Margaret J., Robin W. Pascal, P.K. Taylor, and Bengamin I. Moat. 2009. "AutoFlux: An Autonomous System for the Direct Measurement of the Air-Sea Fluxes." *Journal of Operational Oceanography* 2 (1): 15–23. doi:10.1080/1755876X.2009.11020105.

Yuan, Renmin, Min-Seok Kang, Sung-Bin Park, Jin-Kyu Hong, Dong-Ho Lee, and Joon Kim. 2007. "The Effect of Coordinate Rotation on the Eddy Covariance Flux Estimation in a Hilly KoFlux Forest Catchment." *Korean Journal of Agricultural and Forest Meteorology* 9 (2): 100–108. doi:10.5532/KJAFM.2007.9.2.100.